Graphene on Strontium Titanate

Towards magnetotransport measurements of graphene on $SrTiO_3$

Second master's thesis

of

Dirk van Baarle

Supervisor
prof. dr. J. Aarts

Leiden University
Leiden Institute Of Physics

July 6, 2011

Abstract

The unique electrical properties of graphene make this material to be an interesting system to perform magnetotransport measurements. Phenomena like the quantum Hall effect are studied in detail already, but most of the experiments published do not deal with graphene on substrates with a high dielectric constant. As these kind of substrates will achieve the same charge carrier density in graphene at lower gate voltages, a way to contact graphene on top of these kind of dielectrics is investigated. Several graphene sources and various graphene transfer and deposition methods are compared with each other. A procedure is composed which allows high quality transfer of large areas of graphene from a copper film to another surface. Additionally, a method to deposit electrical contacts on graphene on top of a SiO_2 substrate is developed and the conductivity of the graphene is estimated. Finally the deposition of graphene on STO using mechanical exfoliation is investigated and a method is developed to put high resolution electrical contacts on the insulating STO. Putting all the parts of the reported studies together, a proof of principle is given to contact graphene on STO to perform the desired magnetotransport measurements.

Acknowledgements

At first, I would like to thank professor Jan Aarts who gave me the opportunity to perform my second master internship in his research group. In spite of the fact that I had performed experiments on graphene already (study of graphene synthesis by CVD on transition metals), there was not much similarity between these internships and I've experienced a different physical look at the investigated material. I've been introduced in a total different field of physics. That is exactly the reason why I would like to thank the MSM/AMC group as a whole: thanks for the opportunity to learn about superconductivity, high dielectric materials, molecular conductance etc.

Thanks to my coworkers too. Ji Li, Klara Uhlirova and Ishrat Mubeen in particular. Thanks for the help, patience and input you've given. Marcel Hesselberth, thanks for giving lots of experimental comments and help. Especially thanks to help me to understand and operate the electron beam lithography machine. I appreciate your will to help whenever possible and your critical look at all the procedures I proposed. Finally I would wish Thomas van Tongeren all the best as follow up. Enjoy the time you spend on this amazing graphene and try to get as much physics as possible out of it!

Contents

Chapter 1

Introduction

This thesis contains a summary of the work done during the second internship of my experimental master track. The first chapter gives some background of the internship and the content and structure of the research.

1.1 Goal and structure of the internship

As my first internship was focussed on the growth of graphene, I decided to stick to the same unique material but nevertheless to go to a different field of (interface) physics. To study magnetotransport properties of graphene was chosen to be the main topic of my second internship. In the Magnetic and Superconducting Materials (MSM) group of prof. dr. J. Aarts, much equipment and expertise is available to perform these kind of experiments. Since strontium titanate ($SrTiO_3$ or STO) is a material studied in detail in this group, the goal of my research was to perform transport measurements of graphene on STO, which is a strong dielectric and can be used in gating experiments. But to get contacted graphene on a substrate, experience has to be built up. The plan was to firstly obtain graphene on SiO_2 and subsequently to switch to the STO substrate. In the ideal case, measurements would be performed that show the gating effect of graphene on STO. Low temperature (10 K) and Hall effect measurements were expected to be performed. The following tasks were scheduled to be done:

1. Get graphene on SiO_2.
2. Contact the graphene and measure its mobility.
3. Get graphene on STO.
4. Contact the graphene.
5. Perform magnetotransport measurements.

1.2 Structure of this thesis

The work performed is reported in the following order:

1. The equipment used is listed. The working of Raman spectroscopy is treated in more detail as this was not used in the research group before.
2. The production of graphene is explained and transfer of (commercial) CVD-grown graphene is reported, but no property measurements are

performed because no graphene was found which could be contacted. Mechanical exfoliation is used to produce graphene for further use.
3. Contacting the graphene on SiO_2 by electron beam lithography and the lift-off technique is reported. Initial mobility and resistivity measurements are presented.
4. Deposition of graphene on STO by mechanical exfoliation is reported. First, the optical contrast is discussed and compared with AFM data. Comments are given to contact graphene on STO.
5. Conclusions are made and in the appendix additional information on the paraelectric properties of STO is given. Finally useful experimental procedures are listed.

1.3 Graphene

Graphene is a one atomic thick crystal consisting of carbon atoms. The crystal structure is hexagonal and a large defect-less area of graphene has a lot of unique macroscopic properties. These properties are the reason that much attention is drawn to the (mass) production of graphene.

1.3.1 Graphene production

Since there is no reliable recipe to produce graphene, a huge amount of effort is put in this research field. At this moment, the following two ways of production are used most: mechanical exfoliation (the famous *Scotch tape* method) and growth by chemical vapor deposition. These two methods will be discussed in Chapter 3. They have a very different approach (top down versus bottom up) and only the latter one is scalable to mass production and is promising for the future production of graphene.

1.3.2 Identification of graphene

After the production of graphene, the sample has to be proven to be graphene. The tools that are used to do this are explained in detail in Chapter 2. Especially the optical microscope, the atomic force microscope and the Raman spectrometer are used. As Raman spectroscopy is a quite complicated technique to analyze the graphene, it is treated in detail in chapter 2. One other tool which might reveal information about the thickness of graphene is the Kelvin probe microscope. This kind of microscopy is being introduced in our lab by Hedwig Eerkens. It is used to check whether information could be obtained about the layer thickness of a sample covered with graphene/graphite. Since the measurements are performed by Hedwig Eerkens, the initial results are not reported here.

1.3.3 Transport properties of graphene

Most of the unique properties of graphene are related to its electronic band structure, which is shown in Fig. 1.1. The zoom-in at the Fermi level shows that for (free standing) graphene, the Fermi level intersects at the point where two bands touch each other. At this specific location, the gapless dispersion

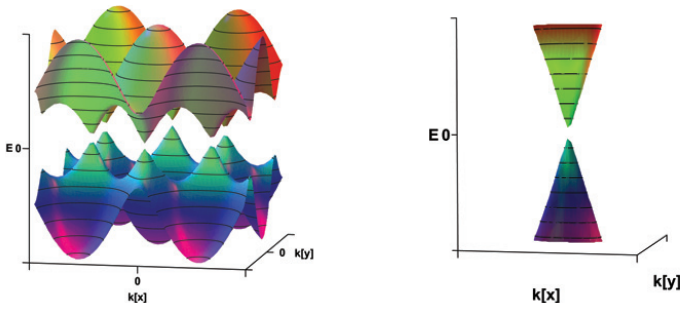

(a) (b)

Figure 1.1: Simulation of the electronic band structure of graphene. The zoom-in shows a detail of one of the six gapless Dirac cones.

relation is almost linear and the electrons behave like massless Dirac fermions. This means that the charge carriers are very mobile, resulting in a very good conductor. Additionally a band gap can be introduced by, for example, the substrate, another graphene layer or induced defects. In this way, the mobility can be tuned and e.g. a field effect transistor behavior can be realized.

To quantify the (electronic) quality of graphene, several methods can be used. The mobility can be checked by looking at the conductivity as function of a back gate voltage. The resulting curve is often used as a fingerprint of the conducting quality of graphene. Monolayer verification of graphene can be done by measuring the (quantum) Hall effect. Only monolayer graphene will show a half-integer quantum Hall effect, while bilayer graphene will show an integer quantum Hall effect [1]. Additionally the influence of different dielectric insulators on the gating effect is interesting to investigate. In this work, SiO_2 and STO are the type of insulators used.

1.4 $SrTiO_3$

Strontium titanate ($SrTiO_3$ or STO) is an oxide crystal having a perovskite structure at room temperature. Undoped STO is a paraeletric insulator with a dielectric constant of about 300 at room temperature. The electrical properties of STO are highly dependent on temperature and on the presence of dopants. E.g. undoped STO has a dielectric constant of about 24000 at 0.3 K [2] but niobium doped STO (Nb-STO) is metallic at room temperature and enters a superconducting state below 1 K. Much research has been performed to understand this behavior. A plot of the experimental data on the dielectric constant of undoped STO as function of temperature, together with a fit using the so-called Barrett formula is shown in Fig. 1.2. The dielectric constant of STO below 10 K is above $20 \cdot 10^3$. Due to this property, a thick STO crystal layer (hundreds of micrometers) can still be used to achieve high electric fields at its surface by applying back a gate voltage. So instead of a 300 nm layer of SiO_2 on Si, a relatively thick layer of STO can be used. On the other hand, as the mobility of graphene is linear dependent on the transverse electric field, it can

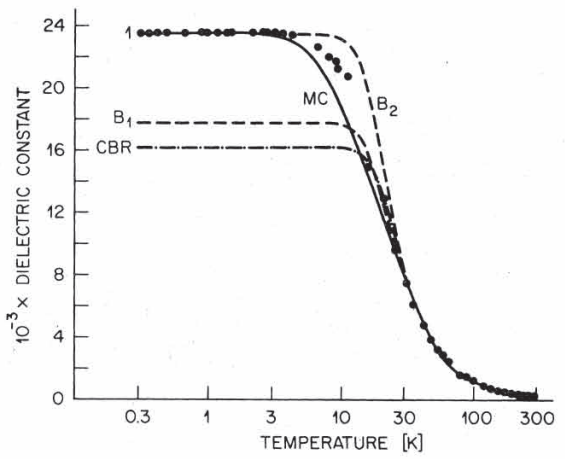

Figure 1.2: Experimental data on the dielectric constant of STO as function of temperature. The data is fitted using several variant of the Barrett formula. Picture token from [2]

be manipulated much more by using insulators with a higher dielectric constant (see Appendix A). Finally, adding dopants to a layer underneath the graphene or STO may result in a very interesting tunable electrical system.

Chapter 2

Experimental equipment

Quite a number of experimental systems have been used to work on the graphene and to make the sample preparation as reliable as possible. In this Chapter, this equipment will be discussed.

2.1 Oxygen plasma cleaner

To remove small (mainly carbon) containing residues from the SiO_2 substrate, the Oxford PlasmaLab 90+ system was used. In this machine, the sample can be loaded in the vacuum chamber using a loadlock. In the vacuum chamber (base pressure $< 1 \cdot 10^{-5}$ mbar) oxygen is introduced and an O_2-plasma is created. The oxygen pressure, the oxygen flow and the power can be set manually.

The O_2-plasma cleaner was not used for the STO substrate since it was not known how the plasma would change the surface.

2.2 Optical microscopy

To perform quick sample inspections and to search for single layer graphene the Nikon eclipse LV150 optical microscope was used. This microscope has a maximum magnification of 1000× and an electrical actuated XY-stage. Additionally several filters are available to enhance contrast and filter specific wavelengths. Together with the eyepiece, the image is recorded by a DS-Qi1Mc-U2 grayscale pixel camera which is connected, together with the XY-stage, to a computer. The camera has a resolution of 1280×1024 pixels and the exposure time can be adjusted to improve the signal to noise ratio. Due to the fact that the camera can only record grayscale images, all optical microscopy images reported in this thesis have a false color scale. All optical microscope images reported have a pink based color scale. The stage and the webcam are controlled by the Nikon NIS-elements v3.07 software.

2.2.1 XY-stage

The movable stage consists of two stepper motors that can move the stage to a desired location within micrometer precision. The camera images are calibrated

at all magnifications. So large area scanning and stitching can be performed at high magnification and, together with a marked sample, the position of local features on the sample can be saved and found back afterwards.

2.2.2 Color filters and diaphragms

In the optical microscope two color filters and two diaphragms are available. The color filters are to balance the color (neutral color balancing filter) and a green interference filter to improve contrast by interference and filter specific wavelengths. The choice for this special green interference filter is investigated and suggested by Blake [3].

The diaphragms available are a field and an aperture diaphragm. The field diaphragm can be used to block stray light to improve the resolution. The aperture diaphragm is used to enhance contrast which improves few layer graphene recognition dramatically. The influence of this filter is demonstrated in section 3.1 and section 5.2.

2.3 AFM

A quite slow but useful technique to measure film thicknesses and to verify the cleanliness of a substrate is the atomic force microscope (AFM). This microscope consists of a cantilever with a small (aspect ratio of 10 nm) tip at its very end. The cantilever with the tip is actuated to oscillate at its resonance frequency. The tip is kept very close to the surface and will have interaction with the substrate by the Van der Waals force. This interaction will change the amplitude of the oscillation. The amplitude is detected by photodiode which measures the reflection of a laser focussed on the oscillating cantilever. Feedback is performed on this signal to keep the amplitude constant by adjusting the height of the cantilever with respect to the surface and thus by keeping the interaction with the surface constant. By scanning over the surface, the height used to create a topographic image of the sample.

Technical data In the work reported here, a Digital Instruments SPM base was used together with the MSM J-scanner (4191JV). This scanner was chosen because it has a lateral range of about 120 μm. The AFM was placed on top of an active vibration isolation platform and inside an acoustic box to improve imaging stability. Non contact mode (tapping mode) was used as probing method. The cantilevers used have a resonance frequency of about 70 kHz. The base was connected to the computer using the DI NanoScope IIIa controller. On the computer, the NanoScope Software v5.30 was installed. Additional image processing was done using the WSxM software. All AFM images reported in this thesis have a color scale which is yellow-red based.

An important and essential tool available in the AFM setup is a 250× magnification optical microscope. With this microscope both the sample and the tip of the AFM can be observed at once. Using the fine XY-adjustment screws of the AFM scanner the tip can be placed at a specific place of the sample within 10 μm accuracy.

2.4 SEM

To investigate the CVD-grown graphene samples a scanning electron microscope (SEM) was used. In this microscope an electron beam consisting of electrons with a specified kinetic energy is focussed on the (more or less conducting) sample. The electrons will interact with the surface: electrons will be scattered back (high energy electrons as it is an elastic process) or will inelastically create secondary electrons (low energy electrons). The intensity of the backscattered electrons carries information about the atomic number of the sample material, the intensity of the secondary electrons has several origins such as the conductivity and the height variations. The image is built by scanning the beam over the surface pixel by pixel. The intensity measured on the electron detector is used to plot pixel in a grayscale image.

The SEM available in the laboratory is a FEI Nanosem 200. This microscope is equipped with an immersion lens to achieve a nanometer resolution. The big advantage of this microscope is that it yields information from the mm-scale up to the nm-scale. The zooming can be done without losing a specific location from the imaging window.

2.5 Raman spectrometer

In this section, Raman spectroscopy is explained in some detail. As it is not straightforward to draw conclusions from spectroscopy data, the physical processes taking place at the sample surface during the experiment are evaluated. At the end, technical data on the spectrometer is presented.

In the next paragraphs, first the fundamental processes are discussed, second the application of the spectrometer to graphene is evaluated. The reported literature study is mainly based on the publications by Pimenta [4] and Saito [5]. Most of the images presented are (rebuilt) copies from these papers. The Pimenta paper gives a nice (but maybe a little outdated) overview while the Saito paper thoroughly discusses the fundamental Raman processes.

2.5.1 Basic principle

A useful analysis tool to determine the quality and the amount of layers of graphene is the Raman spectrometer. It consists of a laser source focussed at the sample and a spectrometer to analyze the photons scattered back from the sample. The elastically and inelastically scattered light is led to a spectrometer and the spectrum around the wavelength of the primary laser beam is analyzed. This light does not only contain the wavelength of the primary beam, but also small intensities of light with a different wavelength. These wavelengths are characterized by their Raman shift (the wavelength shift with respect to the primary beam wavelength). The amount and intensity of the shifts together with the shape of the Raman peaks can be used to determine atomic bonds present in the sample.

Interaction of visible laser light with matter

The way matter interacts with incoming light (or electromagnetic waves in general) is strongly determined by the wavelength of the incoming waves. In the visible spectrum, especially the vibrational modes of the molecules interact with the incoming waves. Another key property of the matter involved, is its polarizability. In the Raman process, the polarizability of the molecule is essential: the higher the polarizability, the more the charges in the molecule will react with the light.

When a molecule interacts with an incoming photon, it absorbs this photon and the molecule will enter an excited state. Depending on the energy of the photon and the energies of the available excited states of the molecule, the photon will excite the molecule to a real or a virtual excited state. After visible light has excited a vibrational molecular state, the resulting virtual state will relax after a certain amount of time to its ground state. The complete relaxation process can be quite complicated, as shown in the next section. For Raman spectroscopy, beside the absorption or emission of phonons, the essential part of the relaxation process is the emission of a photon. The wavelength of this photon is characteristic for the relaxation process. In this way, Raman spectroscopy can be used to obtain a fingerprint of the sample material. The exact relaxation process and Raman signals typical for graphene will be explained later on.

Stokes processes

As indicated, several processes may take place during the relaxation of the system after absorbing a photon. The simplest possible processes are the Stokes processes shown in Fig. 2.1. The main difference between these possibilities is the amount of resonant steps in the process, which makes it a first or second order Raman process.

The first order, one phonon process To start with the most simple case, we begin with the 1-photon emission first order Raman Stokes process, shown in Fig. 2.1A1 and A2. After (1) absorption of the incoming photon (pht, i) of energy $E_{laser} = \hbar\omega_{pht,i}$, the excited molecule can be in a real or virtual excited state with energy $E^1(k) = E_0(k) + \hbar\omega_{pht,i}$. In the first case (real state), the process is called 'incident resonance'. After absorption, (2) an inelastic scattering event results in the creation of a phonon with energy $E_{phn,c}$ and the molecule is left in a *virtual* state with energy $E^2(k) = E^1(k) - \hbar\omega_{phn,c}$. Finally, (3) the molecule will relax to its ground state ($E^3(k) = E_0(k)$) by emission of a photon with energy $E_{pht,e} = E^1(k) - \hbar\omega_{phn,c} - E_0(k)$.

If the molecule is excited in a virtual state ($E(k) = E^1(k)$), the absorption of the photon is called 'scattered resonance'. After absorption, (2) inelastic scattering results in creation of a phonon with momentum q_c and the molecule is left in a *real* state ($E(k) = E^2(k)$). Finally, (3) the molecule will relax to its ground state ($E = E_0^3(k)$) by emission of a photon with energy $E_{pht,e}$.

The second order, one phonon process (double resonance) The four possibilities of the second order, one phonon process are shown in Fig. 2.1B and C. From the schematics it is evident that two resonant transitions and one

virtual state are involved. In the upper schematics (B1 and C1), (1) the absorption is resonant. In Fig. 2.1A, this absorption is followed by (2) resonant inelastic scattering by emission of a phonon with momentum q_c. The molecule is now in a state with energy $E^2(k) = E(k + q_c)$. Then (3) elastic scattering by a defect results in a molecule which is in a virtual state ($E^3(k) = E^2(k)$). This molecule will finally enter its final ground state by emission of a photon with energy $E_{pht,e} = E^3(k) - E_0(k) = E(k + q_c) - E_0(k)$.

In Fig. 2.1B, the resonant absorption is followed by (2) resonant elastic scattering by a defect resulting in a molecular state with momentum $k + q$ and energy $E^2(k+q) = E^1(k)$. After (3) inelastic scattering by emission of a phonon with momentum $q_c = -q$, the molecule will be in a virtual state with energy $E^3(k) = E^2(k+q) - \hbar\omega_{phn,e}$. Finally (4) the electron will go back to its ground state by emitting a photon with energy $E_{pht,e} = E^3(k) - E_0(k)$.

If the molecule is excited in a virtual state with energy $E^1(k)$, two probable ways of decay are shown in Fig. 2.1B2 and C2. In the process shown in Fig. 2.1B2, (2) inelastic scattering by emission of a phonon ($E = E(q)$) brings the molecule in a state with energy $E^2(k + q) = E^1(k) - E(q)$. Now, (3) resonant, elastic scattering by a defect will bring the molecule in the state with momentum k and energy $E^3(k) = E^2(k + q)$. Finally (4) the molecule will enter its ground state by emission of a photon with energy $E_{pht,e} = E^3(k) - E_0(k)$.

On the other hand, the excitation can be followed by (3) elastic defect scattering resulting in the molecule in the momentum $k + q$ state, having the same energy as before: $E^2(k + q) = E^1(k)$. After this, resonant inelastic scattering will bring the molecule in the state with momentum k and energy $E^3(k) = E^2(k + q) - \hbar\omega_{phn,e}$. The phonon emitted has momentum $q_c = -q$. Finally, (4) emission of a photon ($E_{pht,e} = E^3(k) - E_0 k$) will bring the molecule back to its original ground state $E_0(k)$, as shown if Figure 2.1C2.

The second order, two phonon process Two other possibilities that are close to the double resonance, one photon process are the possibilities in which both the (2) and (3) scatter events are *inelastic* and emit a phonon with momentum q and $-q$ respectively. The two possibilities (who differ concerning the position of the real and virtual energy states in the relaxation process) are shown in Fig. 2.1D. Both phonons have to have the same momentum and energy because of momentum and energy conservation.

Anti-Stokes processes

Another category of relaxation processes is valid in the case the initial molecule is not in its ground state but in an excited state ($E = E_1(k)$) at the moment it absorbs a photon. In this case, the absorption of a photon can lead to a stimulated relaxation to the molecular ground state. Because the energy difference between the initial and final state is also released by the photon emission, the emitted photon has *more* energy than the absorbed one. This process is called an anti-Stokes process. Like the Stokes process, the anti-Stokes process itself can be divided into sub-processes too. It is straightforward to derive the anti-Stokes editions of the Stokes processes shown in Fig. 2.1.

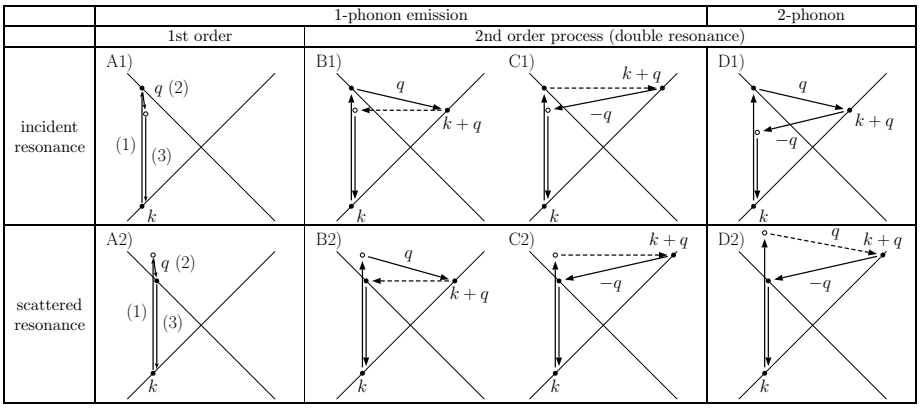

Figure 2.1: Schematic of the most probable Stokes processes. In each schematic, the diagonal lines represent the electron dispersion relation . The phonon(s) created in the electric scattering process are denoted by q. A virtual state is represented by an open circle, a real state by a solid one.

Creation of phonons

A step in the relaxation process which has to be explained in more detail, is the scattering by creation of a phonon (or two phonons). In this step, energy from an excited electron is consumed to create phonons. Due to the fact that this process is elastic, the electron and phonon dispersion relations govern the possible transitions. As these relations are material dependent, from now on the Raman processes will be studied in the case of graphene. For graphene, the electron dispersion relation near the fermi energy (which is linear) is already shown in the schematics in Fig. 2.1. The calculated phonon dispersion relation is shown in Fig. 2.2a. To clarify the situation, the unit cell of graphene in reciprocal space is shown in Fig. 2.2b. As shown, graphene has two sub-lattices. The lattice points are denoted by K and K' for each of these lattices. Because the existence of these sub-lattices, electron scattering can take place inside and in between the sub-lattices. The scattering inside a sub-lattice is often referred to as *intra* valley scattering, while scattering in between the sub-lattices is called *inter* valley scattering. (The name valley is used because of the Dirac cone in the electron dispersion relation near the fermi energy). In the next two paragraphs, these two types of relaxation are explained in the case of single phonon double resonance scattering.

Intra valley scattering In Figure 2.2b, the momentum vector q_{KK} refers to the phonon emitted when intra valley scattering takes place. The vector connects the iso-energy contour belonging to the $k_{initial} = k$-state with the iso-energy contour belonging to the $k_{final} = k + q_{KK}$-state. The electron dispersion relation together with the phonon dispersion relation govern the possible transitions. Note that the vectors q_{KK} connecting those two contours do not have to have the same length.

Inter valley scattering The $q_{KK'}$-vector in Fig. 2.2b shows a possible inter valley process and thus connects two iso-energy contours belonging to the K- and the K'-sub-lattice respectively. It is obvious that these vectors have different

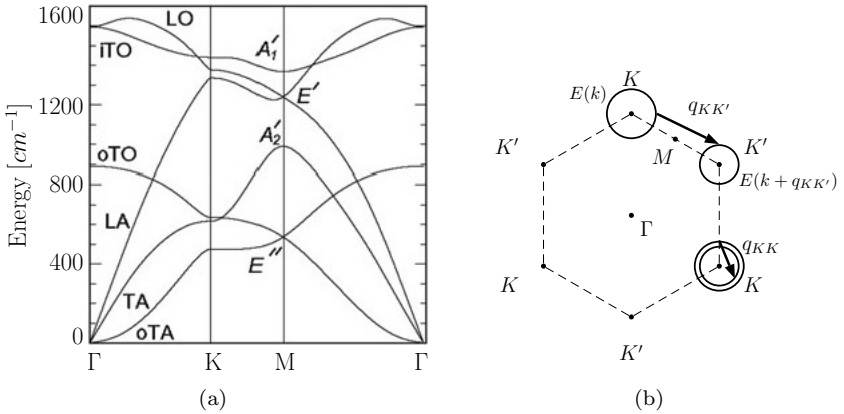

Figure 2.2: (a) Calculated phonon dispersion relation of graphene. (b) Unit cell of graphene in reciprocal space. Iso-energy contours given at certain k_{init}-vectors.

lengths than the q_{KK}-vectors and thus results in a different signal in Raman spectroscopy.

Electron phonon coupling The last question is about which excited electrons do couple to the lattice to create phonons. The electron phonon coupling heavily depends on the specific momentum of both the electron and the phonon. Studies performed by Saito show that Raman spectroscopy can be used to probe phonon branches near the Γ and K points of graphene close the the Brillouin Zone boundary. The emitted Raman phonon intensity as function of $k_{initial}$ and q_{phn} is calculated by Saito and the result is shown in Fig. 2.3a. Remarkable is the laser energy dependence of some signals, indicating which coupling condition is met: $|q_{phn}| = 0$ or $|q_{phn}| = 2|k_{initial} - K|$. In the former case, the electron phonon coupling turns out to be 0. In the latter case, there actually is an electron phonon coupling which leads to observable resonance. Not that in this case, the laser frequency is explicitly involved.

2.5.2 Experimental view on the Raman processes

As shown in all the processes explained above, each relaxation proces involves the emission of a photon. This photon is the information carrier where the Raman spectrometer is based on. Photons reflected by the sample are focussed on a grating and the spectrum of the beam is constructed. The spectrum typically shows a huge intensity peak at the laser frequency: reflected and resonant scattered photons lead to this peak. On both sides of this peak, smaller intensity peaks will appear depending of the interaction of the laser beam with the sample (and the medium just above the sample). The Raman shift defines the position of these peaks relative to the laser frequency peak. This Raman shift

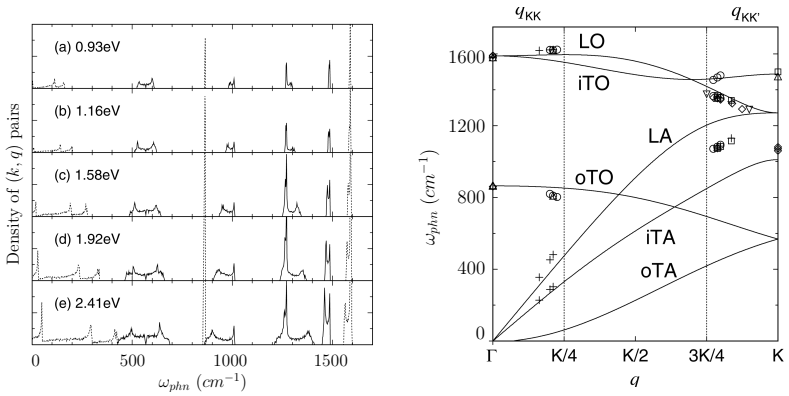

(a) (b)

Figure 2.3: (a) Calculated density of allowed resonance conditions as function of the Raman shift. Calculations are performed at several laser energies. (b) Experimental spectroscopy data compared with the calculated phonon dispersion relation. Only double resonance is taken into account.

will be negative for anti-Stokes and positive for Stokes processes:

$$\begin{aligned} E_{AS} &= E_{pht,i} - E_{pht,e} \\ &= E_{pht,i} - (E_1(k) + E_{pht,i} - E_{phn,e}) \\ &= -E_1(k) + E_{phn,e} \\ &< 0 \end{aligned} \tag{2.1}$$

$$\begin{aligned} E_S &= E_{pht,i} - E_{pht,e} \\ &= E_{pht,i} - (E_{pht,i} - E_{phn,e}) \\ &= E_{phn,e} \\ &> 0 \end{aligned} \tag{2.2}$$

The total Raman spectrum observed gives an overview of all the relaxations of the illuminated molecules. With this information, fingerprints of typical molecular bondings can be recognized and the composition of the sample might by revealed. However, it is not straightforward to couple an observed Raman shift to one specific excitation, scattering and relaxation process. This section will be devoted to use both the electron and phonon dispersion relation of graphene together with the electron-phonon coupling to make a link between the observed Raman shifts and the bonds present in graphene.

Raman-accessible phonon states in graphene

With the knowledge of the Raman processes explained above, calculations are performed to directly link Raman photons to points in the phonon branches. A comparison with experimental data is performed by Saito and the result is shown in Fig. 2.3b. The experimental data fits remarkable well to the calculations.

Comparing all data we can conclude that the following peaks may appear in a typical Raman experiment on graphene:

1. **D-band, 1350 cm^{-1}.** This is a defect induced band which is highly dispersive with respect to the laser frequency: 50 cm^{-1}/eV. The scattering process is the second order, one photon process. It is an inter valley process, so a large phonon wave vector is incorporated in the scattering.
2. **G-band, 1580 cm^{-1}.** This is a double degenerate phonon mode (iTO and LO), Raman active for sp^2 carbon bonds.
3. **D'-band, 1620 cm^{-1}.** A defect induced band, like the D-band. It is a second order, one photon scattering process too. The difference compared with the D-band is the fact that this is a intra valley process, so a small phonon wave vector is present in this process. The laser energy dependence is around 10 cm^{-1}/eV.
4. **G'-band, 2700 cm^{-1}.** This peak is an overtone of the D-band (doubled frequency). The dispersive behavior is about 100 cm^{-1}/eV. This process is a second order, two photon process. Dependent on the actual situation, the signal is a convolution of several peaks. These peaks might contain information of the 3th dimension. The intensity is e.g. very dependent on the layer thickness of the graphene.

Note that not all possible scattering processes are explained above. Important other processes might be involved also, which could clarify the experimental observations in more detail. For example, a tripe resonance might be involved in the process leading to a remarkable strong intensity of the G'-band. Till now, finding explanations of the spectrum being measured is ongoing. Calculations and simulations of other scattering processes possible are part of actual research.

Quantifying the quality

The most common way to quantify Raman data is to evaluate the relative intensity of specific peaks and their relation to a physical property of the sample. In the following paragraphs, several issues will be treated.

1. Graphitic samples have been studied to estimate the crystallite size dependence L_a. The ratio of the D- and G-peaks (I_d/I_g) is very dependent on the laser frequency, but also gives information about the crystallite size dependence. This size can be described in the following way:

$$L_a(\text{nm}) = \frac{560}{E_{laser}^4} \left(\frac{I_D}{I_G} \right)^{-1} \tag{2.3}$$

2. The number of layers of the graphene sample can be coupled to the relative intensity between the G- and G'-peak. A structured study is performed by Wang [6] and one of their results is shown in Fig. 2.4. A rule of the thumb is that if the G'-peak is significantly larger than the G-peak, the sample is single layer graphene. But a comparison between studies shows that experimental results highly depend on the origin of the graphene, the type of substrate and the quality of the spectrometer.

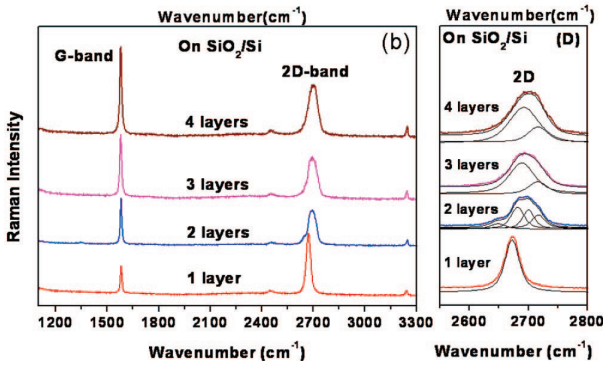

Figure 2.4: Layer dependence of the Raman shift intensities. The change of the composition of the G'-peak is shown also. Image copied from [6]

2.5.3 Technical Data

In this work, the Horiba Jobin Yvon HR800UV Raman spectrometer was used. It is equipped with an optical microscope with a 250× magnification and a manual actuated XY-stage. Three lasers are available: a 442 nm (blue), a 514 nm (green), and a 633 nm (red) laser. The spot sizes of the lasers are about 40 μm^{2}but due to an alignment mismatch between the optical image centre and the laser spot it is very hard to point the laser at a desired location within 100 μm^{2}accuracy. This limits the use of this specific spectrometer to large substrate areas only.

2.6 Electron beam lithography

To deposit the small structures (markers and metallic contacts) an electron beam pattern generator (EBPG) was used in combination with the lift-off technique. To write these structures, a spin coater, a hot plate and a lithography machine are essential equipment.

2.6.1 Spin coater

To write small structures using an electron beam, a sensitive layer has to be put on top of the sample. The most commonly used resists are used: PMMA (with molecular weights 495 and 950) and MMA/MAA. In all the work reported here, a bilayer was used to improve the lift-off. To add a small layer of resist, the sample was centrifuged at high speed after the resist deposition. The spinning was done using a spin coater and the baking was performed using a hot plate.

2.6.2 EBPG

In our lab a Raith e-Line 100 is available, equipped with an XYZ-stage which is actuated in combination with a laser interferometer. With this machine, structures can be written using a resolution of about 20 nm. Structures can be written using an electron beam spot size of <30-700 nm. Because a smaller spot size will result in a smaller beam current, longer exposure times are required.

The electron beam is moved over the sample by deflection coils. These coils are actuated via the electron beam pattern generator. As these coils can induce a limited amount of deflection (with acceptable alignment errors) the writefield area is limited. To be able to write large structures with high resolution, stitching of the writefields is required. This stitching can be done using the movable XYZ-stage. Additional (automatic) alignments can be performed after each stage movement.

To optimize the resolution of the writing, a lot of parameters do matter. The most important ones are the beam current, the area dose, the beam speed, and the area step size. These parameters are dependent on the beam spot size, the substrate and the type of resist. To get known the best values of these settings, dose tests were performed.

2.7 Resistance evaporator

To deposit thin layers of gold on top of the exposed and developed resist, a resistance evaporator was used. In this system, the to be evaporated metal is heated up by driving a large current (up to hundreds of Ampères) through a tungsten boat with the metal on top of it. The sample is exposed to the evaporating metal. Beside the sample a crystal resonator is placed to measure the deposited thickness by the increase of its mass. To improve the quality of the evaporated material, the main chamber of the system is kept at a base pressure of $< 1 \cdot 10^{-7}$ mbar and the sample is introduced using a loadlock. To prevent heating of the resist and sample, a cooled sample holder is used: the sample is kept at about 5 °C.

To improve the contact quality, gold is used. To improve the adhesion between the evaporated gold and the substrate, a chromium layer is deposited. Typical thicknesses deposited are 7 nm of chromium followed by 30 nm of gold.

2.8 Probe station

Because a lot of flakes are tried to be contacted by lithography, an easy and quick way to check these contacted flakes is very helpful. This check is performed using a probe station consisting of a table with microprobes placed inside a Faraday cage. By an optical microscope the probes can be put on 50 μm^{2}sized contact pads. In combination with a computer with LabView software IV-curves of the contacted flakes can be recorded. A Keithly 2400 SourceMeter was used to apply $-150...150$ V back gate voltages.

2.9 Wire bonder

To connect the contacted graphene flakes to the measurement environment, a K&S Convertible dual wire bonder will be used. This system makes it possible to put wires between contact pads on the substrate to a printed circuit board (PCB) for example. Because this technique is only important for measurements of the graphene sample in the PPMS system and these measurements are not

performed in this research, this part of the experiment is prepared (PCB's are made) but not used.

2.10 PPMS

To perform magnetotransport measurements at variable temperature and magnetic fields, a Quantum Design Physical Property Measurement System 6000 is available. In this system a contacted sample can be measured in different circumstances: the temperature can be varied from 4.2 to 300 K and a magnetic field can be applied up to 12 T. Simultaneously the electrical properties can be measured and currents or voltages can be applied using a feedthrough that connects the electrical wires in the vacuum part to the outside world. These measurements are possible because the magnet is placed in liquid helium and the sample is in a small tube inside the magnet with a small heater in it. Together with Ishrat Mubeen leakage current measurements on STO are performed to get familiar with the system. Results of these measurements are not reported here.

Chapter 3

Graphene production

Two methods to obtain graphene on a substrate are reported in this chapter: graphene produced by mechanical exfoliation and the transfer of CVD-grown graphene. These methods are investigated on a Si/SiO_2 substrate. The main question to be answered in this chapter is: what is a reliable way to obtain an identified, micrometer sized graphene flake on SiO_2? Three properties of resulting graphene samples will be discussed in detail:

1. the amount of (multilayer) flakes
2. the cleanness of the flake surface
3. the easiness to localize produced graphene flakes on a substrate

First the mechanical exfoliation method will be discussed.

3.1 Production by mechanical exfoliation on SiO_2

Since the first experimental publications on graphene it is clear that mechanical exfoliation is an amazing easy process to produce micrometer sized flakes of graphene [7][8]. The technique is not suitable for mass production or other automated processes, but for laboratory purposes it is sufficient. Core of the exfoliation process is the cleavage of the graphitic flakes using tape. However, all the steps included in the procedure are investigated to optimize the resulting graphene quality.

3.1.1 Substrate preparation

The substrate used is a bought 4.5 inch n-doped silicon wafer with a 300 nm SiO_2 layer on top of it. After protecting the surface with a polymer, the wafer is cut into pieces of about $5 \times 5\,mm^2$. First, the polymer is removed by putting the substrate in a beaker with acetone in a sonicator. The same is done using 2-propanol (IPA) as solvent. After this treatment the sample is dried using dry N_2 gas. (A detailed recipe can be found in Appendix B.)

O_2 plasma To be sure no carbon containing (organic) contaminants are left on the surface, the sample is cleaned by a reactive oxygen plasma. The plasma will react with all carbon containing particles and form a.o. CO, CO_2 and H_2O. To check whether the influence of this treatment is necessary, AFM images are

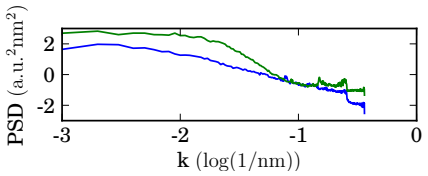

Figure 3.1: A power spectral density comparison of two AFM images made before (blue curve) and after (green curve) application of an oxygen plasma.

made before and after the plasma treatment. The results show a significant increase of the surface quality, as shown in Fig. 3.1: impurities having a lateral radius of several tens of nanometers and a height of a few nanometers are totally removed after the plasma treatment.

Marker deposition After cleaning the substrate a marker field is added on top of it. The exact procedure is explained in chapter 4. In short, a marker field is deposited consisting of crosses with a mutual separation of 200 μm. With this marker field it is possible to localize features with an accuracy of several hundreds of nanometers.

3.1.2 Graphene cleavage and deposition

Directly after the substrate preparation, graphene is deposited using the cleavage method. A highly ordered pyrolytic graphite sample (grade 2) bought from SPI is used as graphene source. First, the graphite surface is cleaned by cleaving off the top layer using tape. The HOPG surface is pushed on a long and clean piece of tape and peeled of. The piece of graphite left on the tape is cleaved and distributed on the tape by folding, gently pressing and unfolding it. This is repeated about 10× while trying to prevent multiple clamping at the same place.

After preparation, the tape is pushed on top of the SiO_2 substrate and pressed in a uniform way. The tape is released gently resulting in a SiO_2 substrate with both pieces from the graphite crystal and tape residue on top of it.

Different kinds of tape The most famous tape used to do mechanical exfoliation is Scotch tape. As some people suggest different tapes work better [9], Nitto tape is used in our work also. Instead of the blue color of the tape mentioned in [9], our Nitto Tape was green-yellow striped. It should result in a higher graphene yield and a lower amount of tape residue.

During exfoliation, the Nitto tape was much harder to handle compared with Scotch tape: the stickiness was much more and parts of the Nitto tape (wire like structures) tend to break apart during unfolding. Additionally it was hard to obtain a dense packed area of graphitic particles. After deposition the optical investigation showed a relatively low yield of promising candidates. On the other hand the amount of tape residue was much smaller compared with the Scotch tape, see Figure 3.2a and 3.2b. In these images, the graphitic patches

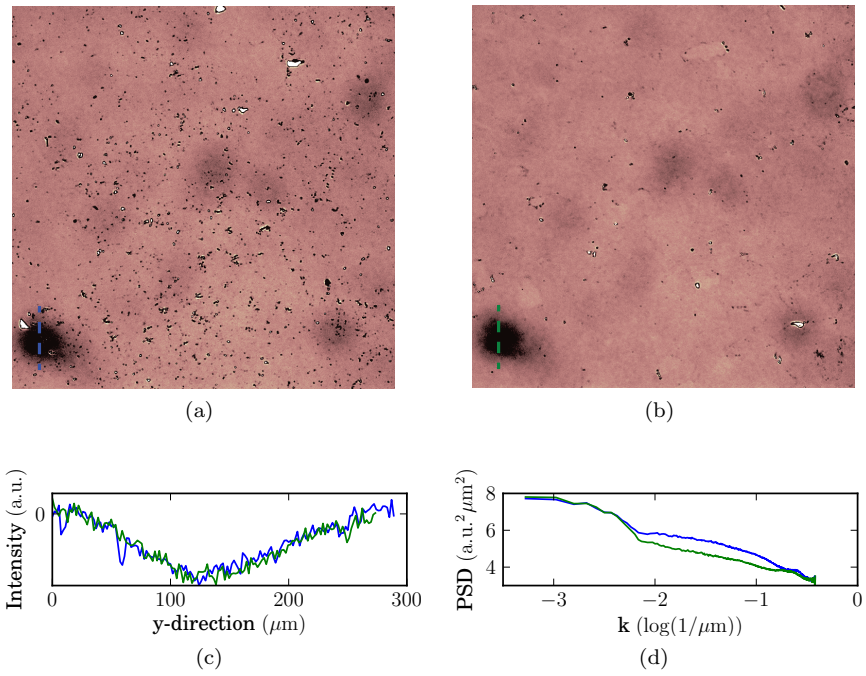

Figure 3.2: (False color) optical microscopy images showing the difference of exfoliation using (a) Scotch and (b) Nitto tape. Image size: $1378 \times 1378\,\mu m^2$. (c) The intensity profile of the indicated lines in the optical image after rescaling the intensity. (d) Power spectral density of both optical images.

are the bright features and the dark structures are tape residue. Using a dirt particle on the lensing system of the microscope, the intensity of the two images is linked (see Figure 3.2c) to compare the power spectral density of both images. The comparison is shown in Fig. 3.2d and clearly indicates that the Scotch tape sample contains more 10-100 μm-sized features, which are mainly contaminants.

3.1.3 Graphene identification and qualification

The appearance of the exfoliated graphite flakes seems to be independent of the kind of tape. In Figure 3.3a and 3.3b two high magnification optical microscope images are shown of cleaved graphite flakes ending up in few layer graphene which are made using different tape.

Surface cleaning To improve the characterization of the graphene flakes, the sample is cleaned from tape residue using chemical solvents. Tetrahydrofuran (C_4H_8O) [10], acetone and IPA are used to do this.

The use of only IPA to decrease the contamination is investigated at samples which were made using the Nitto tape. AFM images of a few layer graphene patch are made before and after the cleaning, see Figure 3.3d. The area scanned

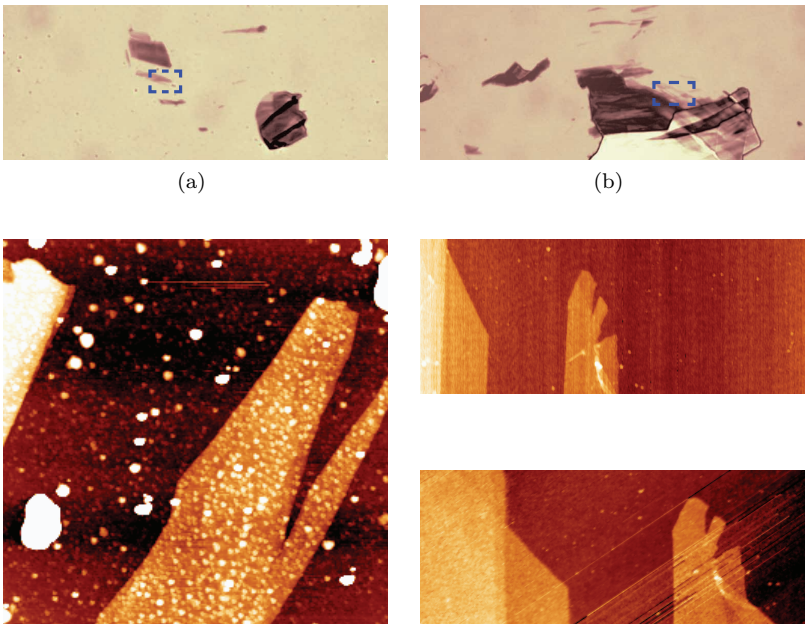

Figure 3.3: (a) Optical microscopy image showing a cleaved piece of graphite after THF cleaning. Image size: $86 \times 35\,\mu m^2$. (b) Optical microscopy image of the Nitto sample after IPA cleaning. Image size: $114 \times 46\,\mu m^2$. (c) AFM image of the in Fig. (a) indicated area. Image size: $5 \times 5\,\mu m^2$; z-scale: 14 nm. (d) AFM images of the area marked in Fig. (b) before and after IPA cleaning. The images are rotated 90° and 148° respectively. Image size $3.8 \times 1.5\,\mu m^2$; z-scale: 12 nm.

by AFM is indicated in the optical image shown in Fig. 3.3b. The influence of the cleaning is not significant. The only complication of the cleaning is a small decrease of the AFM imaging stability, but this might be caused by other parameters like the tip properties too. From this observation it can be concluded that IPA can be used to clean the surface as no new contaminants are observed on the few layer graphene flakes. However, the amount of cleaning is hard to estimate as the initial graphene areas were already quite clean after exfoliation.

As the Scotch tape samples contained a lot of tape residue, THF is used to clean the sample: the sample is put in THF (30 min), acetone (15 min) and IPA (5 min). The result is shown in Fig. 3.3a. The residue is strongly reduced, however, from AFM investigation (Figure 3.3c) of the indicated area in Fig. 3.3a it can be concluded that THF, acetone and IPA are not sufficient to remove the contaminations. Remarkable is the shape of the contaminations: the particles tend to be spherical. This can be explained by the solvent used, which causes the contaminations to minimize their surface area.

Single layer identification

Optical microscopy Initial identification of graphene flakes is done using a standard high magnification optical microscope. However, scanning the whole substrate is a time consuming process. To improve this procedure, studies are performed to understand and improve the contrast graphene causes in optical microscopy [3][11]. These studies show that a green interference filter in combination with a 300 nm SiO_2 layer on silicon is a system that results in a relatively high optical contrast of graphene. Additionally the use of standard optical techniques like aperture diaphragms and field diaphragms enhance the resolution.

To investigate the influence of the optical tricks mentioned above, images are token of the same sample using the different filtering techniques. The results are shown in Fig. 3.4. In Figure 3.4a and 3.4b, no color and interference filtering is used. In Figure 3.4c and 3.4d a green interference filter is placed directly after the light source. Additionally, in Fig. 3.4b and 3.4d the aperture diaphragm is closed at maximum. In the (a) and (c) image, the data scaling is based on the vignetting effect. In the (b) and (d) image, data scaling is based on dirts in the lensing system. This data shows that the green interference filter and the aperture diaphragm improve the contrast dramatically: the graphite containing flat structures show up very differently with compared with the randomly shaped tape residue. In most of the research reported in this thesis, the interference filter and the aperture diaphragm are used intensively.

Raman spectroscopy From Figure 3.3 and 3.4 it can be concluded that optical microscopy is not sufficient to obtain evidence for single layer graphene. Since Raman spectroscopy can give this evidence, the samples are studied by this spectrometer. To do this, the Raman laser has to be focussed exactly at the location identified by the optical microscope. Two issues prevented proper Raman experiments. First, the spot size of the laser is about 40 $\mu m^2$and the flake sizes are typically several microns sized. This means the laser spot (so the photons being analyzed) does not only contain data of the flake, but of its environment also. So there is a difficulty to estimate existence and the quality of single layer graphene single. The second issue has to do with the misalignment of the Raman spectrometer with respect to the optical microscope incorporated in this spectrometer. This misalignment was about 50-100 $\mu m^2$and excluded the possibility of positioning the laser spot on the sample within the desired accuracy. The misalignment can be fixed in the future by accurately measuring the misalignment and by correcting for it using the XY-stage of the microscope.

AFM Another tool to prove the small graphene flakes to be single layer graphene is the AFM. The typical measured thickness of a graphene flake on SiO_2 by AFM is 0.7 nm [12]. In combination with the optical microscope and the markers on the substrate, the AFM is a relatively slow but trustful technique to measure the amount of layers present on a SiO_2 surface.

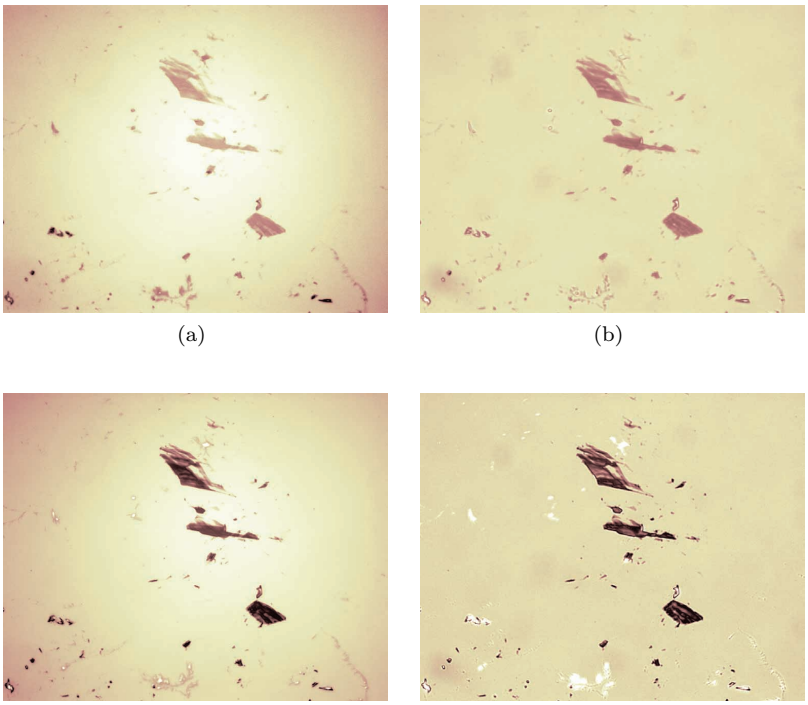

(a) (b) (c) (d)

Figure 3.4: Optical microscopy images showing filtering effects: (a) no filtering; (b) aperture diaphragm closed; (c) green interference filter, aperture diaphragm open; (d) green interference filter, aperture diaphragm closed. Image size: $115 \times 92\,\mu m^2$.

3.1.4 Conclusions

Cleavage mechanisms

To optimize the graphene quality and to understand the results of the additional cleaning steps, the question raises: what exactly happens at the moment of cleavage? What is the role of contaminants? During exfoliation, two possible events are possible to take place during each time the squeezing sides are retracted: either a graphite flake splits in two parts, resulting in two flakes on each part of the tape, or a graphite flake sticks as a whole on one of the sides. In the first case the part of the graphite exposed to the air is fresh and just cleaved, in the latter case the graphite side facing the air has been exposed to the tape. This is schematically shown in Fig. 3.5. The difference between these two events concerning the amount of tape contamination is quite evident: in the former case almost no contaminants are expected to be present on the graphite surface, in the latter case lots of residue is expected to be left on top of the graphite surface. The extreme differences in surface quality of the few layer graphene flakes shown in Fig. 3.3 can be understood with this explanation: in Fig. 3.3c the flake was totally released from the tape, while the other AFM image (Figure 3.3d) suggests cleavage took place during deposition.

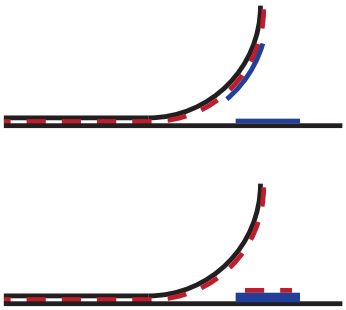

Figure 3.5: Schematic view of the exfoliation process (red color represents tape residue, blue color represents the graphite flake). Either the graphite flake is cleaved, or the flake is released from the tape. In the first case almost no tape residue is left on the cleaved surface.

Optimal recipe to find single layer graphene

The obtained knowledge lead to the following optimal exfoliation procedure. First, the substrate has to be cleaned by an oxygen plasma. Second, the density of flakes on the tape should be as high as possible. Third, clean graphene flakes are expected to be located near 'cleaved' large area patches. These cleaved parts are expected not to have tape residue on top. This last item is not a very strict conclusion but this rule of the thumb will increase the success rate of finding graphene. A last issue is the need of the AFM which is essential to determine the quality of the graphene flake after its localization by optical microscopy.

3.2 Harvesting CVD-grown graphene

After the increase of attention to graphene, lot of research is done on scaling the production of it. One of the most promising production methods is the growth of graphene on transition metals. The growth is done by deposition of carbon containing molecules on the metal surface at elevated temperature, the so called carbon vapor deposition (CVD) method. The result of this technique is a metal film (which might be a very thin film deposited on top of another substrate) covered with graphene. The properties of the grown graphene are very dependent on the type of metal and the growth procedure. In this section, the properties of CVD grown graphene are investigated. Additionally a method is developed to perform the transfer of graphene to a SiO_2/Si substrate. A proof of principle is shown to transfer large area CVD grown graphene to any desired substrate.

3.2.1 Graphene sources

In the work reported here, two graphene sources have been used: graphene grown on a nickel film deposited on an oxidized silicon substrate and graphene grown on a thin copper sheet. Both sources are bought via *www.graphene-supermarket.com*. Before transferring the graphene, the samples are investigated thoroughly by several microscopes and the copper grown graphene is investigated by Raman spectroscopy too.

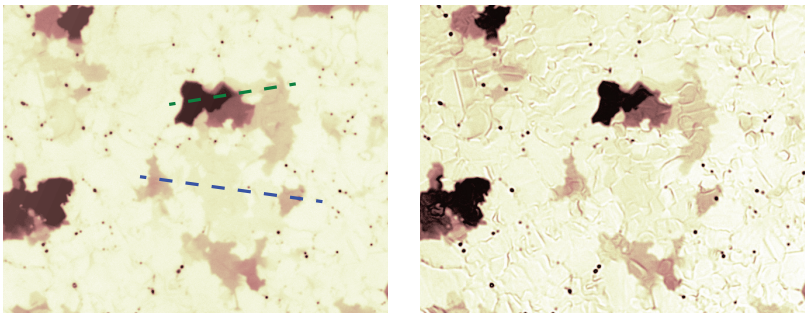

(a) (b)

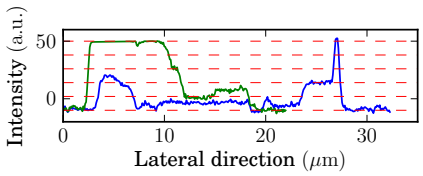

(c)

Figure 3.6: OM images of graphene on nickel (a) without and (b) with using the aperture diaphragm. Image size: $59 \times 47\,\mu m^2$. (c) Height profiles of the indicated lines in Fig. (a). Equidistant red lines indicate the possibility of graphene layer counting.

3.2.2 Graphene grown on a nickel film

Optical microscopy

At first, graphene grown on nickel is investigated by optical microscopy. The influence on the contrast of switching the green interference filter should not be major as there is no interference effect of graphene and SiO_2. As expected, the *contrast* is not enhanced by switching this filter. Nevertheless, a minor improvement of the resolution is observed. This can be explained by the blocking of stray light which very well could be frequency dependent. The influence of the aperture diaphragm is shown in Fig. 3.6a and 3.6b. Remarkable is a new structure/roughness appearing when using the diaphragm. This suggests the (nickel) surface is very rough, which can be quite well explained by polycrystalline domains of the deposited nickel film. More evidence for this is obtained by AFM and SEM, as presented further on.

In Figure 3.6c two intensity profiles of Figure 3.6a are shown. After equalizing the background signal, the intensity profiles show terraces of equal intensity. In the graph shown, equidistant guides for the eye are plotted indicating each even amount of graphene layers. These lines demonstrate that the intensity difference between consecutive layers is constant which can be explained by the absorption of light by the graphene layers. As the nickel film is highly reflective, each light ray hits each graphene layer twice on its path and doing so, it doubles the effect of light absorption. So a reflective substrate will improve the contrast and the countability of graphene layers.

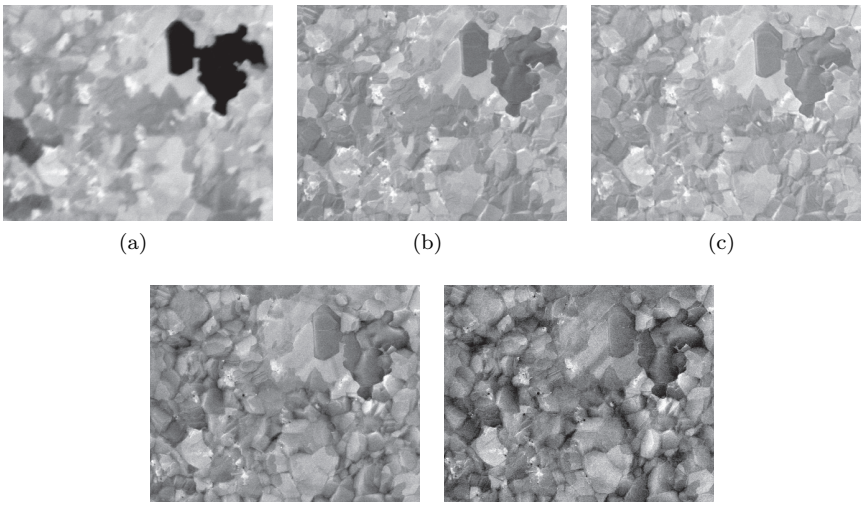

Figure 3.7: SEM images token at the same location of graphene grown on a nickel film at different primary beam energies: 2 kV, 5 kV, 10 kV, 18 kV and 30 kV respectively. Image size: $27 \times 24\,\mu\mathrm{m}^2$.

SEM

To obtain more information about the surface structure of the graphene-nickel samples, SEM images are made. A thorough understanding of the physical processes taking place during scanning is required to prevent misinterpretations. One of the most important parameters in this process is the primary beam voltage. In the SEM, high energy primary electrons approach the surface and interaction with the surface results in the creation of secondary electrons. The higher the energy of the incoming electrons, the larger the penetration depth of those electrons. So more subsurface information will be present in data obtained using high energy primary electrons, while surface (graphene) information will be obtained if a low energy is used. The influence of this energy dependence for the graphene-nickel sample is shown in Fig. 3.7. From these results it is evident that the amount of secondary electrons created locally is more uniform at lower primary beam energies.

In the 2 kV image, discrete intensity steps are visible suggesting the influence of the graphene thickness on the secondary electron creation. This has some resemblance with the optical images made, but a comparison of a $100\,\mu\mathrm{m}^2$sized SEM image with an optical image does not give evidence of countable graphene layers: there are too much other features (impurities and subsurface influences) that frustrate this attempt. This results in the conclusion that the SEM is not the best tool to perform layer estimation of graphene on a polycrystalline nickel film.

The 30 kV image gives subsurface information about the shape of the nickel crystallites underneath the graphene. Different orientations of the crystallite

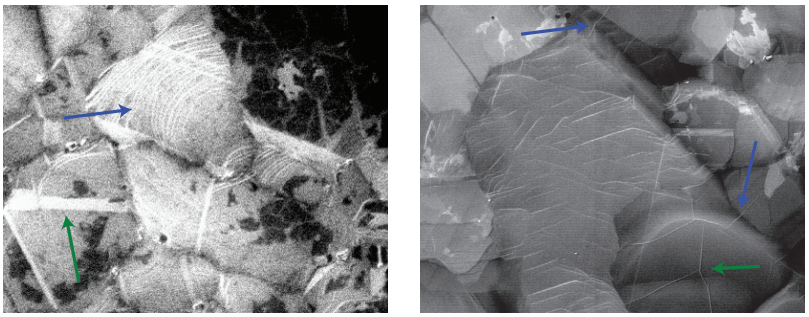

(a) (b)

Figure 3.8: SEM images of graphene on nickel (a) without and (b) with graphene on top. Primary beam voltage: 30 kV. Image sizes: (a) $7.3 \times 5.9\,\mu m^2$; (b) $9.9 \times 7.9\,\mu m^2$.

with respect to the primary electrons results in different yields of secondary electrons. This explaines the 3-dimensional appearance of the SEM image. As no constant intensity plateaus are observed, no evidence for graphene can be obtain from this data.

Graphene growth and quality aspects High magnification imaging is performed to search for features that have a different yield of secondary electrons. These features might give information about the graphene quality and insight on the graphene formation might be obtained. Some images of this investigation are shown in Fig. 3.8. In these images, the difference is visible between an area which is not covered with graphene and an area which is covered. On the uncovered area (Figure 3.8a), some of the crystallites have rounded shapes and bunches of atomic steps decorate the surface (indicated by the blue arrow). The flat crystallites present do have sharp corners with dominant 60 and 120 ° angles reflecting the crystalline structure of nickel. The sides of the flat crystallites show large step edges, indicated by the green arrow. These step edges are expected to be the result of the conglomeration of a bunch of steps which is energetically favorable.

Evidence of the presence of an additional surface layer on top of the nickel is obtained form Figure 3.8b. The arrows plotted, point at lines that are expected to be cracks in graphene. These lines are not present *in* the nickel surface, but *on top* of it, as shown by the cracks highlighted by the blue arrows. These cross nickel crystallite borders, so they are present in a surface layer on top of the nickel. Another indication for the presence of graphene is the different shape of the crystallites with respect to the not covered areas. On the graphene covered area almost no curved shapes are visible. This indicates that graphene makes the crystallites more stable by lowering the mobility of the nickel atoms (remind that the growth takes place at high temperatures of around 1000 K).

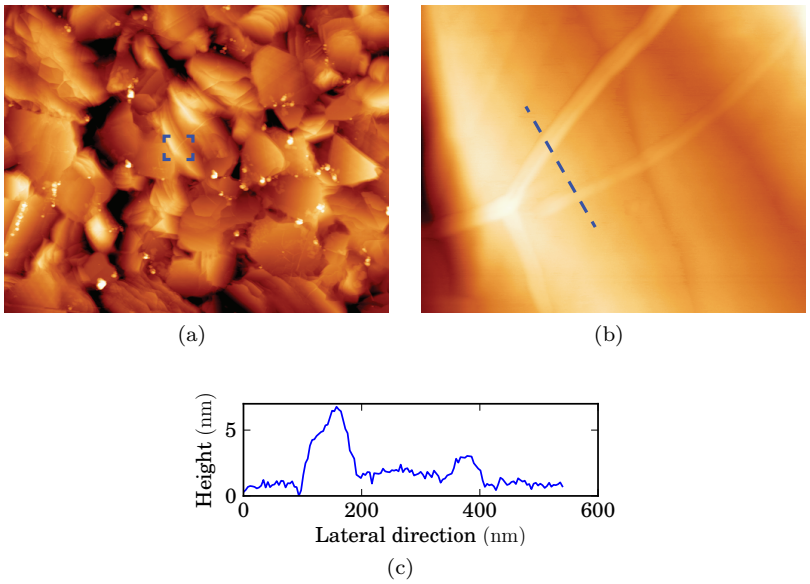

Figure 3.9: (a) AFM image of the with graphene covered polycrystalline nickel film. Image size: $20 \times 16\,\mu m^2$; z-scale: 150 nm. (b) Zoom in of the indicated area in Fig. (a) showing a graphene ripple. Image size: $1.6 \times 1.3\,\mu m^2$; z-scale: 56 nm. (c) Height profile of the indicated line in (b).

AFM

The way graphene is positioned on top of the nickel polycrystalline surface is studied by AFM. The result is shown in Fig. 3.9. This data shows that the surface structure does correspond with the structure observed in high-kV SEM images. The ripples observed by SEM are observed by AFM too. A detailed image of such a ripple is shown in Fig. 3.9b. The height profile of this ripple (Figure 3.6c) shows that the height of those ripples is in the order of nanometers. As the graphene single layer thickness is about 0.7 nm on SiO_2 on can conclude that those ripples are relatively high, folded pieces of graphene. An origin of those ripples could be the thermal expansion difference between nickel and graphene which will cause stress during the cooling down of the sample after growth [13].

3.2.3 Graphene grown on a copper film

Optical microscopy

In the optical microscope, the graphene on copper sample looks very different with respect to the nickel sample. Two typical images are shown in Fig. 3.10a. In the lower magnification image straight lines are visible originating from the roll-to-roll fabrication of the polycrystalline copper film. Additionally a structure is present that divides the film in multiple domains. A higher magnification image of these domains (Figure 3.10b) shows that different surface structures can be observed in different domains. These are expected to be the crystallites

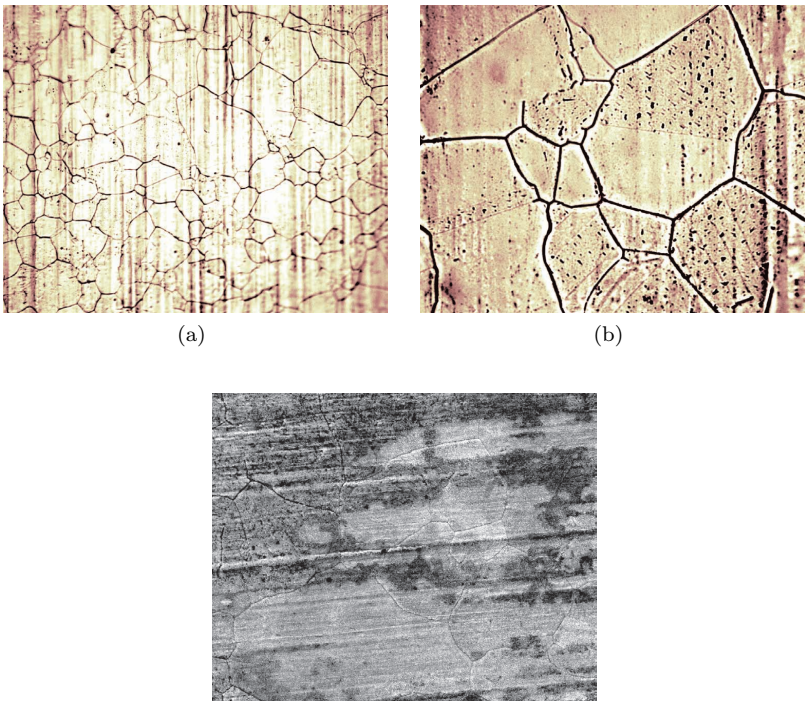

Figure 3.10: (a) Low and (b) high magnification optical images of a bought polycrystalline copper film with graphene. Image sizes: (a)$1.1 \times 0.9\,\mathrm{mm}^2$; (b) $115 \times 92\,\mu\mathrm{m}^2$. (c) SEM image of a typical area of the sample used in (a) and (b). Image info: size $250 \times 200\,\mu\mathrm{m}^2$; primary beam voltage: 30 kV.

which grow when the high temperatures are applied to grow graphene (close to 1300 K). But more evidence is needed to justify this conclusion. No structure is observed which suggests the presence of graphene.

SEM

From SEM experiments, no evidence is found for graphene too. In the investigation (typical image shown in Fig. 3.10c), no major primary electron beam dependence is observed and no additional structures are detected that resemble with published observations [14][15]. Features that are observed can not be linked with the presence graphene.

Raman spectroscopy

To prove the evidence of single layer graphene on the copper film, the sample is investigated by the Raman spectrometer. Using the green laser (514 nm) the film is scanned searching for a G'-peak. During this scanning, almost no signal around the expected G'-peak at $2700\,\mathrm{cm}^{-1}$ is observed. At a few spots, some signal was observed but it was very weak. This indicates that the quality of the graphene (size, defects) which might be present is quite bad.

3.2.4 Conclusions on the as-grown graphene quality

The study of the graphene grown on a nickel film yields the following conclusions:

1. The layer thickness of the graphene can be determined by the optical microscope. The green interference filter optimizes the contrast between layer thicknesses.
2. The nickel crystallites underneath the graphene result in a high surface roughness. Graphene follows the nickel surface morphology and overgrows the crystal domains. This behavior corresponds with literature very well [15][16].
3. In the graphene, ripples are observed. These ripples extend over domain boundaries and prove that the graphene flakes have sizes larger than the substrate crystallites. They might originate from thermal expansion coefficient difference with respect to the nickel substrate during the graphene synthesis.

According to the observations of the graphene on copper sample it can be concluded that almost no graphene is present. Nevertheless, graphene synthesized on copper is expected to be a very promising graphene source. The bought sample was a very bad quality sample: no successful growth was achieved. Improvement of the growth procedure is required.

Graphene quality

The results reported show that it is hard to obtain large sized high quality single layer graphene flakes. The size of the single layer flakes grown on nickel is quite reasonable (up to $10\,\mu m^2$) but the quality of those flakes are expected not to be very good based on their morphology. Additionally, the transfer of the 3-dimensional shaped graphene to a flat surface might induce ripples. These aspects will decrease the quality of the magnetotransport measurements. So graphene grown on nickel is not a promising candidate to deliver samples to perform magnetotransport studies. The quality of graphene grown on a copper film can not be estimated from the sample used in this work as no reasonable amount of graphene is found.

3.3 Graphene transfer method

To prepare the transfer of graphene from the metal films, experiments are performed to optimize this transfer method. The ultimate goal is to get graphene from a transition metal (nickel, copper) to an insulating surface (SiO_2, STO) while the quality of the initial graphene is maintained.

Initial sketch of the transfer process

To transfer graphene from a metal to another (insulating) surface, two major steps have to be taken: the removal of the metal and the deposition of the graphene on the new substrate. Several issues will take an important role:

- The impact of the etchant on the graphene.
- The manipulation of graphene after removing the metal substrate.
- The purification of graphene on the new substrate?

These questions will be dealt with during the discussion of the complete transfer method.

3.3.1 Final transfer method

To keep things clear, the final recipe to transfer graphene is given here and the steps chosen are discussed afterwards. In this way the structure of the investigation will be evident and relevant issues will be presented in an well ordered way. The recipe which results in high quality transfer of graphene consists of the following steps (a detailed recipe is given in the appendix):

1. Cover the graphene on one side of the metal with PMMA resist.
2. In case of a metal sheet: apply an O_2 plasma to the sample while the backside is facing up.
3. Coat the graphene/PMMA side with a thick (around 40 μm or more) layer of SU-8 resist.
4. Put the resist-side on Scotch tape (see Figure 3.11c).
5. Etch the metal by a $FeCl_3$/HCl solution.
6. Dip the sample in de-ionized water.
7. Dip the sample in a 10× diluted 38% HCl solution.
8. Dip the sample in de-ionized water.
9. Dry the sample using a dry N_2 flow.
10. Press the graphene on the new substrate.
11. Remove the tape by adding a droplet acetone.
12. Immediately dip the sample in acetone.
13. Transfer the sample to fresh acetone and keep it there for 15 min.
14. Dip the sample in IPA and put it in fresh IPA for 5 min.
15. Dry the sample using dry N_2.
16. Bake the sample for 15 min at 110 °C.

3.3.2 Discussion and results on the investigation of the transfer method

The recipe presented will be discussed in the following way: first the need of the oxygen plasma is explained, second the handling of graphene during the transfer will be evaluated, third the etching procedure will be explained and finally the treatment after deposition will be discussed.

Oxygen plasma A first item is the use of the O_2 plasma in step 2 of the process. This step is performed to remove the graphene which might be present at the back side of the metal foil: during CVD growth, both sides of the metal foil are exposed to the process gasses used to grow graphene, so both sides will be covered with graphene. To remove the graphene at the back side, PMMA is deposited at the front side to protect the graphene and O_2 plasma is used to remove the graphene at the back side.

Etching and cleaning In the work reported here, an 0.5 M $FeCl_3$ and 0.01 M HCl solution is used as etchant. This is favored with respect to concentrated HCl as this produces bubbles at the etched interface which will destroy the graphene film. The etching takes about 45 mins, after which the sample is washed in

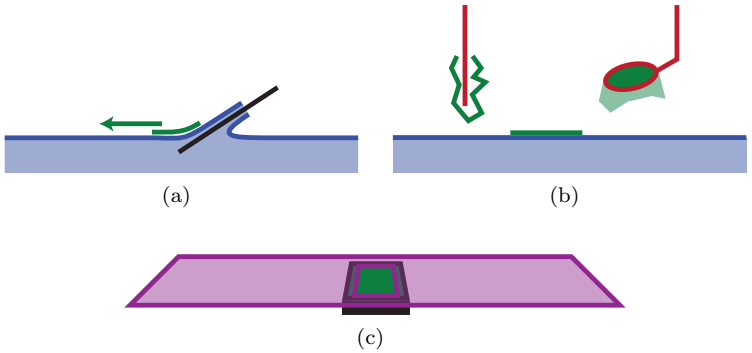

Figure 3.11: Schematic view several steps of the graphene transfer process. (a) Problem of the surface tension pushing the graphene away. (b) Importance of a proper shaped stick to lift the grahene. (c) Sketch of the SiO_2/graphene/PMMA/SU-8 underneath the tape with a hole in it. (colors: blue = solution, black = SiO_2 substrate, green = graphene, purple = tape).

de-ionized water and put in a 38% HCl solution to remove residual metal ions. The sample is washed twice in de-ionized water afterwards and is dried using a dry N_2 flow.

Graphene handling during transfer

A critical issue in the graphene transfer is the way how the graphene is treated after the metal substrate is removed. It is very small and flat, so damage can be induced easily. Several methods investigated to solve this issue are listed here.

Metal-graphene-SiO_2 A first approach is to press the metal on the SiO_2 substrate with the graphene in between and to etch away the metal. However, the roughness of the graphene on the metal is quite much resulting in a minimal amount of contact between graphene and SiO_2. The etchant can easily get in between the graphene and the SiO_2 preventing the increase of the contact area. This method is not promising and is not tested.

Catch by SiO_2 A second approach is to transfer graphene to the SiO_2 by moving the silicon substrate in the etchant to catch some flakes. As the graphene is hydrophobic, it floats on top of the etch solution and should be easy to catch. However, two issues turned out to be a problem: first, the graphene flakes are small and hart to find and second, due to surface tension and the hydrophilic nature of SiO_2 the solution tends to stick to the substrate and the graphene is pushed away. This is schematically shown in Fig. 3.11a. This method is quite ill controlled.

Transfer stick To make it easier to catch the graphene, a (platinum) rod can be used to take the material out of the solution. The shape of the stick is important, as a conventional stick or tweezer will allow the graphene to wrap itself around the stick resulting in a lot of cracks preventing proper deposition. A stick with a ring-like structure (see Figure 3.11b) solves this problem, however,

because the edges of the graphene are wrapped around the ring, a simple release is not possible. Putting a SiO_2 wafer underneath the ring which fits into the ring followed by dropping the ring and pushing the graphene on the substrate does not solve the problem: it is hard to get the graphene loose from the ring and a lot of stress, ripples and incisions are created. So the use of a stick does not work.

Adding carrier layer The graphene on the metal is not one large continuous layer, so small flakes will float on the etching solution once the metal is etched away. A polymer deposited on top of the graphene before etching solves this. Two types of polymer are investigated: PMMA (polymethylmethacrylate) and SU-8. Because one single layer of PMMA was expected to be too thin and fragile, SU-8 is used as an additional supporting layer on top of the PMMA. In this way the graphene layers will be quite stiff and easy to handle. After successful transfer, it turned out that the SU-8 carrier (without the PMMA interlayer) resulted in more contaminated samples compared to the carrier with PMMA included. This might be explained by the adhesion between the polymer and the graphene: it is suggested that the adhesion between SU-8 and graphene is much more due to the presence of the benzene-like rings present in both graphene and SU-8.

Scotch tape To prevent the graphene to wrap around the transfer stick, the metal/graphene/PMMA/SU-8 sample is put on top of Scotch tape. After pressing the SU-8 side on the tape, the tape is used as a carrier which can be handled easily without applying stress to the graphene. After etching, the sample is pressed on top of the SiO_2 substrate followed by the release of the tape. The release is done by acetone. To minimize the amount of tape dissolved, a hole is made in the tape before putting on top of the SU-8/PMMA/graphene/metal. A schematic view is shown in Fig. 3.11c. The tape can be released easily by adding a droplet of acetone on top of the SU-8. The U-8 will dissolve and the sample left can be moved further using tweezers.

Treatment after deposition

After the deposition of the acetone to release the Scotch tape, the sample has to be put in acetone immediately. In case the deposited acetone is evaporated before the sample is put in the acetone solution, the resist present on the sample becomes harder and more difficult to remove. After the sample is put in acetone, the resist dissolves in about one minute. The sample is transferred to fresh acetone and is kept in it for 15 min to ensure that all resist is removed. Next, the sample is dipped in IPA for 10 min. After drying the sample with dry N_2 gas, the sample is baked for 15 min to evaporate water left and to increase the adhesion between graphene and the SiO_2 substrate.

3.3.3 Results on the graphene transfer

In this section microscopy and spectroscopy data is presented showing the importance of specific entries in the transfer process. Although the nickel and copper samples are shown to be low quality graphene sources, useful information on the transfer procedure is obtained.

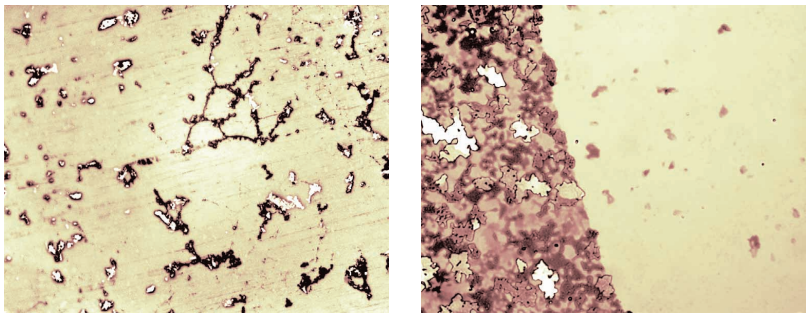

(a) (b)

Figure 3.12: Result of graphene transfer from the (a) copper and (b) nickel substrate. Image size: $115 \times 92\,\mu\text{m}^2$.

The first proof of success which has to be given is that material originating from the metal substrate is transferred to the SiO_2 surface. A clear indication of this is presented in Fig. 3.12a. This optical microscope image of a SiO_2 surface after transferring graphene from a copper foil shows the structures which were present on the copper foil. The transfer is done using PMMA and the sample is put in acetone for a very short time, so the PMMA film is still present. Comparison of this image with Figure 3.10b shows that both the domain boundaries of the crystallites and the straight lines originating from the production process of the foil are visible. The domain boundaries behave like 'garbage bins' during high temperature annealing and this material is successfully transferred.

An optical image of graphene transferred from nickel is shown if Figure 3.12b. PMMA is used as a carrier. This image shows that a complete sheet of (multi-layer) graphene is transferred. It is evident that it is hard to obtain single layer graphene from these samples.

These observations lead to the conclusion that material from the metal surface is transferred a the new substrate. It is very assumable that graphene on top of the copper foil, in case it is present, will be transferred also. More evidence of the successful transfer of graphene is given in the next paragraph.

Quality of transferred graphene To estimate the quality and cleanness of the transferred graphene, extensive Raman investigation is performed. Due to the misalignment of the laser beam with respect to the optical microscope inside the system, it was not possible to take a spectrum of a small specific area. The samples were moved while the spectrum around the G'-peak was being analyzed. A complete spectrum was made in case a G'-peak was found.

In Figure 3.13, typical Raman data of graphene transferred from copper is presented. In all spectra, the signal which originates from the SiO_2 substrate (around $1000\,\text{nm}^{-1}$) is used as a calibration signal. The blue curve shows the spectrum of an empty area of the substrate. The peaks observed originate from

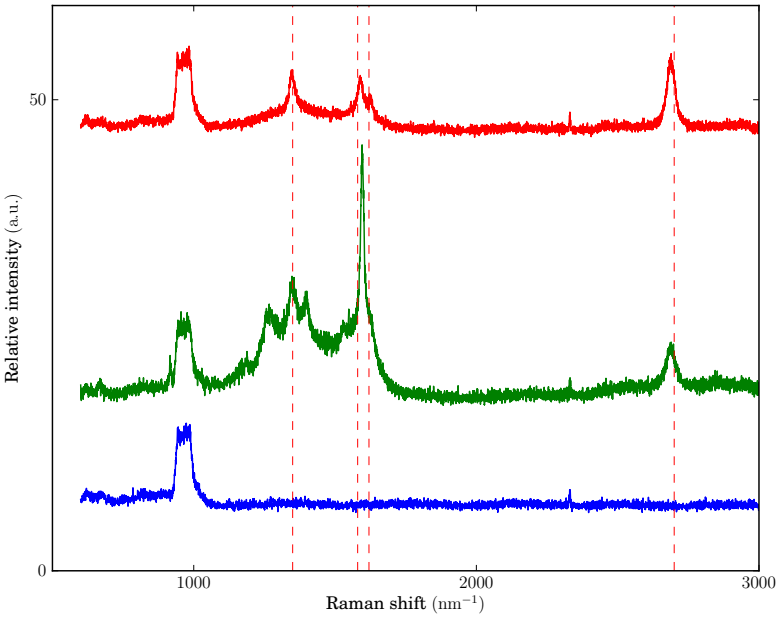

Figure 3.13: Raman spectra of graphene transferred from copper to SiO_2 using a 514 nm laser. Blue curve: empty silicon substrate covered with a 300 nm SiO_2 layer. Green curve: area covered with graphene, transfer done using SU-8 as carrier. Red curve: area covered with graphene, transfer done using PMMA/SU-8 as carrier.

the substrate and the air (the N_2 peak at 2330 nm^{-1}). The green curve is the spectrum of graphene transferred using SU-8 as a carrier. The intensity of the G'-peak is relatively low which indicates that the graphene is not a monolayer. However, this is unlikely as the growth procedure should produce monolayer graphene only. A more likely explanation is that the 40 μm laser beam is illuminating the edge of a flake. This will decrease the G'-peak and the large signal around the D-band indicates the low quality of the graphene observed which might be the edge of the flake. Additionally, as SU-8 contains a lot of carbon and benzene bonds, the presence of this material will result in a D and G-band signal too.

The red curve in 3.13 represents the Raman data obtained from graphene which is transferred using the PMMA/SU-8 carrier. The result is very promising: not only the G'-peak is much higher than the G-peak, but the intensity of the D-band is low with respect to the green curve. So the conclusion can be drawn that the flake being analyzed is a quite clean single layer graphene patch. As this area was very small and quite unique, an increase of the yield of graphene is required. Nevertheless, the data presented proves that the transfer process performed works perfectly.

3.4 Summarized conclusions

After the evaluation of several techniques to obtain graphene which is ready to be contacted, we can draw the following conclusions.

The cleavage mechanism yields usable graphene flakes which are located near and at the ultimate end of cleaved, larger graphite patches. Due to the fact that these single layer flakes are located near those large patches, they are relatively easy to find. The surface of the graphene will be very clean in case the cleavage took place in the deposition/tape release step. To identify single layer graphene easily, a green interference filter and the aperture diaphragm are essential tools in the optical microscope.

Graphene grown on a metal surface is only useful in case it is large area, single layer graphene. On nickel the majority of the graphene is multilayer, but the single layer graphene grown on polycrystalline copper is a promising source. The graphene coverage and the impurities on the copper surface are key issues to obtain large areas of high quality graphene samples. A successful and high quality transfer process is developed to transfer graphene from a metal to a SiO_2 substrate.

Chapter 4

Contacting graphene on insulating surfaces

After deposition of graphene on the insulating substrate, the sample has to be contacted in order to perform magnetotransport measurements, which is described in this chapter. First the desired quality of the contact structure and the accuracy of the location where it has to be written is discussed. Second the recipe to deposit alignment markers and the contacts is presented. The first transport measurements are presented also.

4.1 Requirements

4.1.1 Contacts

The structure needed to perform magnetotransport measurements is the Hall bar structure. A schematic top view of this structure is shown in Fig. 4.1. Applying a current via contacts A and B, measuring the voltage across contacts C and D and applying a back gate voltage yields the data to calculate the resistance and mobility of the graphene. Measuring the voltage between C and E under application of a magnetic field perpendicular to the surface yields the Hall voltage.

To suppress the influence of local features on the sample and to demonstrate the large scale properties of high quality graphene, the Hall bar should be as large as possible. However, as the graphene flakes produced by mechanical exfoliation are typically quite small, a size of 1 μm is chosen for the minimum Hall bar length. From this choice, the main requirement on the structure is that it has to be possible to create contact paths with a width and a mutual distance of about 300 nm, which has to be done by electron beam lithography.

4.1.2 Markers

Another requirement is the accuracy to deposit the structure at the desired location. This is very dependent on the size of the graphene too: in case the graphene is covering large areas, it is not critical. Since the samples used in

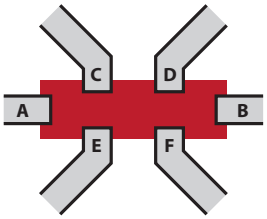

Figure 4.1: Schematic of the Hall bar which allows Hall effect measurements. The grey traces are the contacts, the red area represents a graphene flake.

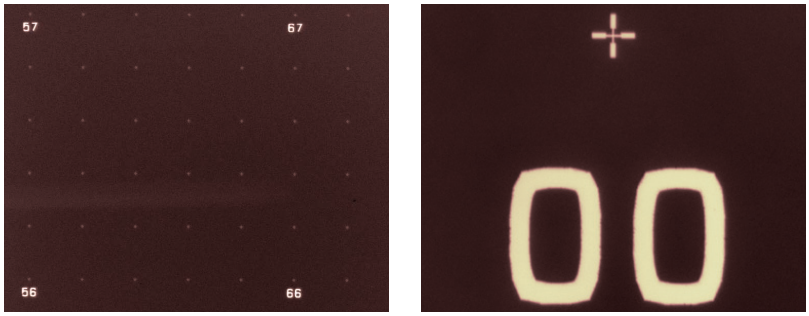

(a) (b)

Figure 4.2: (a) Overview of the marker pattern on SiO_2. (b) High magnification image of the marker field origin. Image sizes: (a) $1.5 \times 1.2\,\mathrm{mm}^2$, (b) $92 \times 73\,\mu\mathrm{m}^2$.

this research contain graphene deposited by mechanical exfoliation, graphene is rarely present on the surface and a procedure has to be used that allows to find back the small graphene flake.

To determine the exact location of a flake, a marker field is added on top of the substrate. An overview and a zoom in of such a field is shown in Fig. 4.2. It consists of a grid with $10\,\mu$m sized crosses placed at a mutual distance of $200\,\mu$m. The mutual distance of $200\,\mu$m makes it possible to have at least one complete $200 \times 200\,\mu\mathrm{m}^2$ square visible by the optical microscope of the AFM, so AFM investigation on a specific flake is possible. Additionally, the $10\,\mu$m sized crosses are can be used to optimize the EBPG alignment: before the contacts are written, the stage is moved towards the center of the square in which the graphene flake is present. The markers will be scanned automatically and alignment of the beam is performed, after which the contacts are written.

As the substrate has an surface area of $1\,\mathrm{cm}^2$, it is time consuming to find back a specific square by counting the small markers. To avoid this, an additional grid is added: each millimeter, the millimeter coordinates of the X- and Y-direction are written in large size (each number height is about $40\,\mu$m , see Figure 4.2b). For example, the left bottom corner of the first millimeter sized square is “00” and one millimeter further in the X-direction, it is “10”. This allows us to roughly align the substrate by a low magnification optical microscope.

4.2 Methods

4.2.1 Writing markers

As the quality of the marker field is very important to obtain accurate alignment, electron beam lithography in combination with gold evaporation and the lift-off technique is used. An overview of the procedure used to deposit markers is listed here, a detailed list is put in Appendix B.

Write lift-off structure

1. Prepare a $1 \times 1\,\mathrm{cm}^2$ SiO_2 substrate (O_2 plasma cleaning included).
2. Deposit a bilayer of MMA/MAA (300 nm) and PMMA-495 (300 nm).
3. Write a $8 \times 8\,\mathrm{mm}^2$ marker field (crosses) using the following writing parameters:
   - spot size: 110 nm
   - area dose: $200\,\mu\mathrm{C/cm}^2$
4. Write the text using the following writing parameters:
   - spot size: 200 nm
   - area dose: $140\,\mu\mathrm{C/cm}^2$
5. Develop the resist by dipping the substrate in MIBK:IPA 1:3 for 45 sec.
6. Dip the substrate in IPA (after-develop) for 45 sec.
7. Dry the substrate suing a dry N_2 flow.

Deposit metal

8. Clean the substrate in an O_2-plasma for 100 sec.
9. Deposit a 15 nm layer of chromium and a 35 nm layer by evaporation.

Perform lift-off

10. Dip the substrate in acetone for 30 min.
11. Rinse with acetone.
12. Dip the substrate in fresh acetone for 2 hour.
13. Dip the substrate in IPA for 1 min.
14. Put the substrate in IPA for 10 min.
15. Dry the substrate using dry N_2.
16. Clean the substrate using an O_2-plasma for 5 min.

A typical result of this recipe is shown in Fig. 4.2. Several important details are discussed below.

Resist preparation The deposition procedure of the bilayer resist is very important in order to obtain high resolution by a proper lift-off. Two issues are investigated: the kind of bilayer and the baking procedure. Both a bilayer of 200 nm PMMA-950 on top of 300 nm MMA(8.5)MAA and a bilayer of 200 nm PMMA-950 on top of 200 nm PMMA-495 have been used. The PMMA bilayer, using baking at 180 °C for 1 min, did not result in an easy and high quality lift-off: large areas of the unexposed resist did not lift off. Next, MMA/MAA was used as first layer (which should result in a larger undercut), the baking procedure was changed to 170 °C for 20 min (to ensure uniform baking) and a water cooled sample holder was used during the metal evaporation. This resulted in a successful lift-off and a good marker resolution as shown in Fig. 4.2.

Figure 4.3: Schematics of two different types of metal deposition: metal evaporation and ion sputter deposition. The substrate is covered with a bilayer resist (the green and blue bars).

Writing parameters For the quality of the markers and the text, the writing parameters are not that crucial. A dose test was performed to estimate the best exposure dose. An area dose of 200 μC/cm^2 produced the best quality for the markers. For the text, a slightly smaller dose was required as the exposure of large areas had a more significant proximity effect. An area dose of 140 μC/cm^2 resulted in a good quality.

A more important issue during writing is the stability of the beam. As the area of the marker field is quite large, exposing this area takes its time due to all the stage movements. During time, the properties (beam current) of the electron beam will change slightly and the exposure will change. To prevent quality loss, every 15 min the beam current was measured and the exposure parameters (area dwell time) were corrected automatically. As the optimization of the writing parameters for the markers led to a total writing time of 15 min per substrate, this correction was only performed in between the writing of the marker-layer and the text-layer. The text does not have to be written at high resolution, so by using a relatively large beam size of 200 nm the writing time was reduced to 5 min.

Resist development The development procedure contains one important parameter: the length of the time the sample is put in the developer solution. This length will be determined by the minimum development time required to sufficiently dissolve the exposed areas and the maximal time before the undercut of MMA underneath the PMMA starts to be too large and a collapse or removal of the PMMA starts. The minimum and maximum development time are estimated to be 45 and 90 sec respectively. Developing for 60 sec resulted in an undercut of about 100-200 nm.

Metal deposition The metal was deposited using evaporation by resistive heating. As explained in the equipment chapter, the metal source is placed in a tungsten boat which is heated until the metal starts to evaporate. The metal leaves the boat in a straight way. This is the reason why metal evaporation is preferred to sputtering deposition: in the latter technique, the plasma contains ionic particles which moves in all directions. The effect of the bilayer resist with the undercut at its edges is not as effective as in the evaporation case (see Figure 4.3): in the metal evaporation system, the upper layer of the resist will cause a shadow of the metal beam and no metal will be deposited underneath the undercut.

As the adhesion of gold on SiO_2 is not optimal, chromium was used as an adhesion layer. On top of this layer, gold was used as the actual contact material. The desired thickness of the these layers is determined by the requirements of

a continuous chromium layer and the visibility of the structures by optical microscopy. Deposition of several thicknesses led to the conclusion that in practice a bilayer of Cr:Au 7:35 nm was used.

4.2.2 Writing contacts

To write contacts on a localized graphene flake, rougly the same recipe as writing the markers is used. The differences are listed and discussed below.

Preparation of the resist

The sample preparation to write the structures is equal to the marker field writing preparation, except for the oxygen cleaning step. Since the oxygen plasma reacts with all carbon containing molecules, graphene will be removed too.

Software design

To write the contacts exactly on top of a specific flake, its coordinates have to be transferred to the EBPG. In the work reported, this is done using the import of optical microscope images to the marker field design in the EBPG software. The optical microscope image is prepared in such a way that it has no rotation and at least one marker is in it. This image is imported in the EBPG software using the coordinate of the marker and the image size. So the software knows the exact location of the graphene flake with respect to the origin of the marker field. After calibration of the EBPG-stage with respect to the marker field on the substrate (origin and rotation) the machine can drive to the flake.

After importing the optical image, the Hall bar structure is drawn on top of the image. As the graphene is visible in the image, this drawing is relatively easy. The Hall bar structure is magnified depending on the graphene size. To prevent distortion of the geometry of the Hall bar, the structure is put inside one single writefield. So no stage movements have to be performed while writing the Hall bar.

Traces To prevent overexposed spots in the Hall bar structure, the first contact traces are connected to the Hall bar without any overlap and do have the same width (300 nm). To prevent significant influence of the trace resistivity, these traces have a limited length of 5 μm. A second issue is that the time allowed to write those structures is limited, as temperature drift will distort the symmetry of the Hall bar. This temperature drift is observed to be significant, as a writing of the individual structures the wrong order caused a deformation of the Hall bar.

The small 300 nm traces are connected to the traces which go to the contact pads by intermediate width (1 μm) traces, see Figure 4.4. At the place the 300 nm trace connects to the 1 μm trace, a square is written to ensure the connection.

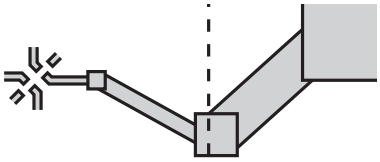

Figure 4.4: Schematic lay-out of one of the traces. The length of the traces is not in proportion to the thickness. At the left hand side the Hall bar structure is plotted, at the right hand side a part of the contact pad is visible. 300 nm, 1 μm and 10 μm traces connect a contact of the Hall bar to the contact pad. The dashed line represents the border of the writefield consisting of the Hall bar and the small traces.

Contact pads The contact pads and the traces connecting the contact pads to the 1 μm traces are designed as a separate layer because they require a higher resolution. Each contact pad has a size of $100\times200\,\mu m^2$ and is connected to the small trace by a 10 μm trace. Again, a square ensures the connection of the traces, as shown in Fig. 4.4.

Writing parameters As mentioned in the previous paragraph, the small and large structures are written using different resolution. In this way the writing speed is optimized, the thermal drift is minimized and the beam instability in time is not significant. Based on this layout, the following writing parameters are used: //for the detailed structure:

- spot size: 41 nm
- beam current: 0.03 nA
- area step size: 6.3 nm
- area dose: 200 μC/sec
- beam speed: 2.5 mm/sec (calculated by software)
- area dwell time: 3 μsec (calculated by software)
- total writing time: 15 min

for the large structure:

- spot size: 700 nm
- beam current: 3.99 nA
- area step size: 88 nm
- area dose: 200 μC/sec
- beam speed: 22.6 mm/sec (calculated by software)
- area dwell time: 4 μsec (calculated by software)
- total writing time: 5 min

At a small spot size, the beam speed is kept below 5 mm/sec in order to prevent distortions at small scale. In case the beam speed is higher, the electron beam is not stable enough to obtain high quality high resolution structures.

Alignment To write the structures at the desired locations with sub micrometer accuracy, three of the four markers around the graphene flake are used to optimize the beam alignment. The markers are scanned by the software automatically and feedback is performed to optimize the beam deflection (rotation, translation and shear correction). The alignment is repeated until the error is below 50 nm.

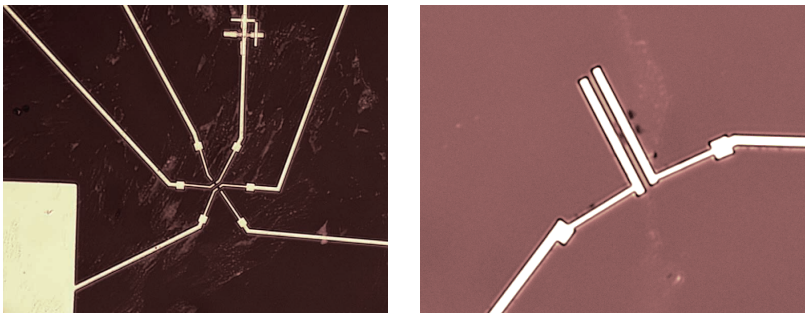

(a) (b)

Figure 4.5: (a) Optical microscopy image of gold contacts to measure the Hall effect. (b) Image of gold contacts on top of a multilayer graphene flake. Image sizes: (a) $98 \times 79\,\mu m^2$; (b) $43 \times 35\,\mu m^2$.

Development and evaporation

The resist development and metal evaporation procedure is almost identical to the marker field deposition procedure. The only difference is that no oxygen plasma can be used and thus the cleaning by IPA has to be very precise in order to reduce the amount of contaminations on top of the graphene.

4.3 Contact writing results

The method discussed above results in high quality Hall bars which can be easily connected to external instruments by the wirebonder or the probe station. A high magnification optical microscopy image is shown in Fig. 4.5a. This image demonstrates the perfect symmetry of the written Hall bar. It illustrates the alignment lines on top of the alignment marker too. Due to an alignment error made by the user, the structure was not on top of a flake, so no magnetotransport measurements were performed using this sample.

4.4 Initial resistivity measurements of graphene on SiO_2

Despite the fact that contacting single layer graphene was unsuccessful, a multilayer graphene area is contacted by two electrodes to perform standard mobility and resistivity measurements. The electrodes are placed 950 nm from each other. By measuring the effect of the application of a back gate voltage, a rough estimate can be made about the thickness of the graphene/graphite flake: no gate effect will be present and a linear IV-curve is expected in case the flake is graphitic.

The flake, with gold electrodes on top, is shown in Fig. 4.5b. The n-doped silicon wafer with the 300 nm SiO_2 layer is put on top of a metal plate and silver paint is used to ensure electrical connection between the metal and the

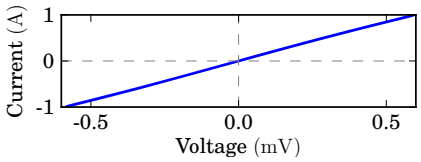

Figure 4.6: Typical measured IV-curve of the contacted flake in shown in Fig. 4.5b. The slope of the curve is 1.71 kV/A.

silicon. This metal plate is used as contact pad for the back electrode. After transferring this system to the probe station, electrical probes are put onto the connection pads and two-probe IV-curves are recorded at different back gate voltages. The back gate voltage is varied from $-100...100$ V in steps of 10 V and -150 and 150 V are applied. An influence of the back gate on the conductivity of the flake is not observed. All IV-curves were identical and a representative curve is shown in Fig. 4.6. This curve shows a perfect linear behavior. So the flake measured behaves classically at room temperature and its resistivity is estimated to be 1.71 kΩ. Using AFM, the average thickness and with of the flake are estimated to be 6 nm and 3 μm respectively, so the electrical resistance is about $3.2{\cdot}10^{-5}$ Ω·m). This resistance is comparable with the reported in plane electrical resistivity of graphite (10^{-6} Ω·m range) [17]. As no additional treatments are applied to improve the conductivity of the flake and to lower the contact resistance, the result is reasonable.

4.5 Conclusions

A method was developed to contact graphene flakes on SiO_2 wafers. Flakes with a minimal size of 2 μm (or even 1 μm might do) are required.

The electrical connection between the electrodes and the graphite/graphene was demonstrated by performing a mobility and resistivity measurement on a multilayer graphene area. No back gate voltage dependence is observed and the IV-curves were linear, yielding a resistivity of $3.2{\cdot}10^{-5}$ Ω·m. The classical behavior of the sample at room temperature indicates that the sample was a multilayer area of graphene: it has a graphitic behavior.

Chapter 5

Graphene on $SrTiO_3$

As the final goal of this research project is to measure magnetotransport properties of graphene on $SrTiO_3$ (STO), the deposition and identification of graphene on STO is investigated. In this chapter, the relevant properties of the STO substrate and the cleaning of STO are discussed. After that, issues conerning electron beam lithography on STO are reported and finally the identification of graphene deposited by mechanical exfoliation is presented.

5.1 Sample preparation

5.1.1 $SrTiO_3$ substrate properties

Thickness In the case that $SrTiO_3$ (STO) single crystal substrates are used as a dielectric between the back gate electrode and graphene, the thickness is an important parameter. Together with the dielectric constant it defines the charge density in the conducting (graphene) channel at a certain gate voltage (see Appendix A). The thinner the dielectric, the lower the gate voltage and the higher the minimal temperature required to achieve a specific charge density in the graphene. The gate voltage and temperature constraints are determined by the PPMS: the available voltage range is $-150...150\,\mathrm{V}$ and the lowest temperature achievable is $4.2\,\mathrm{K}$. As explained in Appendix A, these constraints result in a maximal STO thickness of $500\,\mu\mathrm{m}$. The minimal STO thickness is limited by the risks of leak currents and the breaking the substrate. STO thicknesses of $100\,\mu\mathrm{m}$ and $500\,\mu\mathrm{m}^2$ are chosen. To prevent breaking of the substrate during resist deposition and mechanical exfoliation, a substrate holder was designed which clamps the STO substrate to a holder by applying low vacuum from the back side.

Surface polishing An atomically flat STO surface is required to obtain an homogeneous electric field at the interface between STO and graphene. So the graphene is deposited on a polished STO surface. For practical reasons, the $100\,\mu\mathrm{m}$ thick STO substrate used was polished on both sides.

Surface orientation The surface orientation of STO in the experiments reported is (100). The miscut of the surface normal is $< 0.1\,^\circ$ for both substrate

thicknesses and an additional 500 μm thick sample is used having a 1 $^\circ$ miscut.

5.1.2 STO cleaning and resist deposition

The as-delivered STO is packed in a special box to ensure no contaminations will be deposited during transport and storage. To avoid introducing contaminants on the STO, the substrate is only blown clean with dry N_2. Optical investigation showed that the surface did not contain visible contaminants.

The STO surface is covered with a bilayer resist of 300 nm PMMA-950 on top of 300 nm MMA(8.5)/MAA. The same procedure is used as in the SiO_2 case, apart from the use of the special designed sample holder that results in more stability during spinning.

5.1.3 Marker field and contacts deposition

To localize graphene and to align the EBPG to write the electrical contacts accurately, a marker field is deposited on the STO surface. As the substrate is insulating, local charging of the substrate is observed during the focussing and the writefield alignment. This charging effect is less in case a smaller spot size (41 nm, so a smaller current) of the electron beam is used. Additionally, this effect dramatically increases the first few seconds of exposure. This makes the charging less significant in the writing mode of the EBPG, but makes the charging very significant during the manual focussing and alignment procedures. To still be able to perform proper focussing and writefield alignment, the edge of the STO sample is used. There the contrast between the STO and the base plate of the EBPG is enough to perform adequate focussing and alignment.

Deposition of contacts

A dose test is performed to see whether the required resolution could be reached to write 300 nm bars with a mutual distance of 300 nm on STO. A dose of 175 μC/cm^2 results in underexposure, a dose of 225 μC/cm^2 causes an overexposure which leads to a to the risk of having electrical connection of the by 300 nm separated bars. A dose of 200 μC/cm^2 resulted in the best quality.

The surface charging might be an issue in case automatic alignment on predeposited alignment markers is required to deposit contacts on graphene. This was not investigated in detail, but the use of small spot sizes (low beam current) and the short beam exposure during these alignment scans might suppress the charging problems. At least it is certain that no manual alignments are possible on the STO surface. The deformation of the electron beam observed during imaging suggests that the minimal accuracy of the position of the contacts on the substrate is about 5-10 μm.

Writing parameters

The following parameters were used to write the marker field:

- spot size: 110 nm (alignment markers); 320 nm (text)
- area dose: 200 μC/cm^2 (alignment markers); 175 nm (text)

To write the 300 nm bars, the same settings are used as for writing the Hall bar contacts on SiO_2. As explained, The area dose of 200 μC/cm^2 is very critical.

After development of the resist, the same procedure is following as in the SiO_2 case, except the use of the oxygen plasma since it was not known whether a reactive oxygen plasma will change the surface structure of the atomically flat STO.

5.1.4 Graphene deposition by mechanical exfoliation

On top of the written marker field, graphene is deposited using mechanical exfoliation. The other deposition methods are not investigated as there were no good CVD samples available. Damage to the thin STO during the release of the tape was tried to be prevented by the special designed sample holder. This worked well for the 500 μm thick STO, but the strong adhesion of the Scotch tape forced the 100 μm thick STO sample to bend and break.

5.2 Graphene identification

The way to find single layer graphene on the STO surface is not studied much yet. Other work already shows that the optical contrast of graphene on STO is not very good [18]. In the following paragraph an attempt is made to couple optical and atomic force microscopy data in order to simplify the identification of graphene by optical microscopy. As in the case of SiO_2, patches of multilayer graphene having cleaved edges are studied in detail.

5.2.1 Optical vs atomic force microscopy

In Fig. 5.1, two optical microscopy images are shown which demonstrate the improve of the contrast of the few layer graphene in case the green interference filter is used. In both images, the diaphragm aperture is applied to improve the resolution further. The STO substrate is a 500 μm thick, one side polished sample. An AFM image of the same area is shown in Fig. 5.1c. The thinnest areas are estimated to be bilayer graphene. One of these areas is indicated by the blue arrow.

A comparison of the optical and the atomic force microscope images lead to the conclusion that the optical contrast of few layer graphene is very small. It is not possible to identify the bilayer areas. One might argue that the sizes of the bilayer pieces present are too small to be observed by optical microscopy. But the fact that a 1 or 2 μm^2 piece of few layer graphene can not be observed, shows that the optical microscope is a very limited tool to investigate graphene on STO.

5.2.2 Contaminants on graphene surface

In case optical microscopy cannot be used to locate graphene, AFM seems to be the best tool. However, it is not possible to scan large areas by AFM: it is very time consuming and contaminations will damage the AFM tip. A way to solve

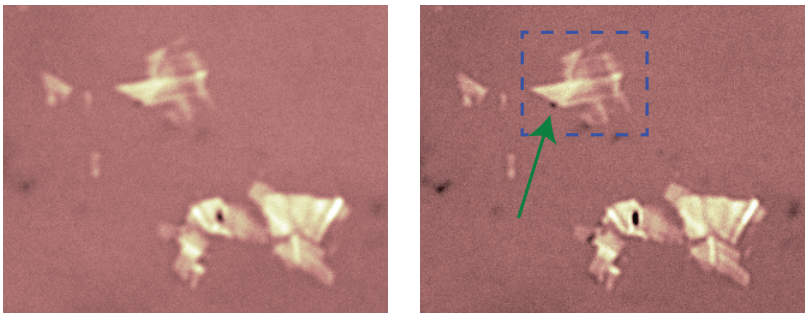

(a) (b)

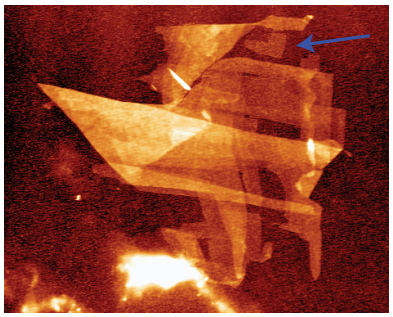

(c)

Figure 5.1: (a) and (b): Optical microscopy images of a cleaved part of graphite on STO. Images made using the aperture diaphragm and the green interference filter is used in Fig. (b). Image sizes: $29 \times 23\,\mu\text{m}^2$. (c) Atomic force microscopy image of the patch indicated in Fig. (b). Image size: $9 \times 7.4\,\mu\text{m}^2$, z-scale: 11 nm.

this issue is to use the optical microscope to search for cleaved graphite patches and investigate whether surface contaminations are present on the graphene. Two reasons are in favor of this approach: first, it is very probable to find graphene near or at the edge of cleaved graphite patches. Second, up to $1\,\mu$m sized contaminations are able to be observed by the optical microscope because they show up differently compared with the very flat graphite areas. Especially the green interference filter and the aperture diaphragm result in a very different behavior of the contaminants. This can be seen in the images shown in Fig. 5.1: a contaminating particle is observed by the optical microscope indicated by the green arrow in Fig. 5.1b. This particle is much less visible in the optical image without the use of green interference filter (Figure 5.1a) and the AFM image shows that the size of this particle is about $1\,\mu$m. So the optical microscope can still be used to estimate locations where it is very probable to find graphene, AFM can be used to perform further, more detailed investigation.

5.2.3 Single layer identification

An example of an AFM image of single layer graphene flakes on top of STO is given in Fig. 5.2a. The substrate is $500\,\mu$m STO with a miscut of $1\,^\circ$.

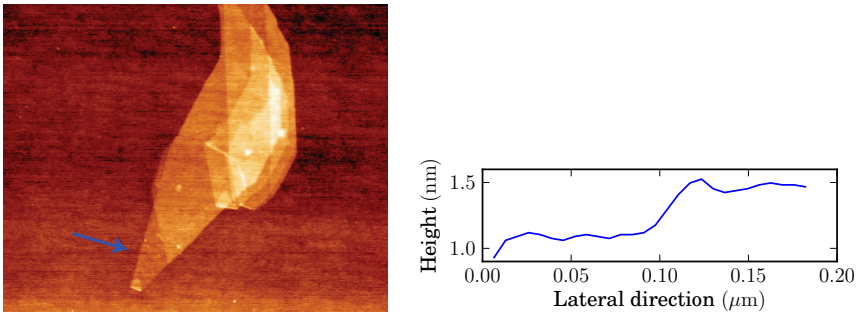

(a) (b)

Figure 5.2: (a) Atomic force microscopy image of a cleaved part of graphite ending in a piece of single layer graphene in the left bottom corner. Image size: $3.1 \times 2.5\,\mu m^2$, z-scale: 3.4 nm. (b) An over 17 height lines average of the step edge indicated with the blue arrow.

The terrace steps of the STO surface are visible. In the bottom left corner, a thin piece of graphene is located and statistics of one of the steps between the graphene layer and the substrate yield a step height of 0.38 ± 0.06 nm (see Figure 5.2b). This resembles quite well with literature (on STO, a single layer graphene height of 0.34 ± 0.01 nm is reported by Akcöltekin).

5.3 Conclusions

The investigation of graphene on STO reported here shows that the optical contrast between few layer graphene and the STO substrate is not sufficient to identify single layer graphene. Nevertheless, the optical microscope is necessary to find cleaved areas which are very probable to have single layer graphene at the edges. Additionally micron sized contaminations can be identified also.

Atomic force microscopy is used to estimate the layer thickness of few layer graphene areas. In this way single layer areas are found on STO. The single layer step height is estimated to be 0.38 ± 0.06 nm, which corresponds very well with literature.

Comments for future graphene research on STO

The most important conclusion for further work is that it is very well possible to obtain graphene on STO. But the way to obtain graphene to perform the experiments required, is by mechanical exfoliation. First, it is very inefficient: mechanical exfoliation is a very unpredictable process and it is time consuming to find promising candidates by optical microscopy and to prove the single layer property by atomic force microscopy. Second, the charging of the surface during the electron beam exposure introduces alignment errors. This will prevent to deposit contacts on a located, micron-sized graphene flake. In short, each electron beam exposure step introduces errors due to charging of the surface.

These two issues are both connected to the graphene source: mechanical exfoliation. In case graphene is put on top of STO by the transfer of high

quality CVD grown graphene, almost the complete surface will be covered by single layer graphene. So no marker field is required and lots of large sized contacts can be deposited straightforwardly. Additionally the charging effect is expected to be less because the electrons can distribute themselves over the surface through the graphene itself. Thus the experiments lead to the conclusion that large area graphene is needed to contact single layer graphene on STO.

Chapter 6

Conclusions

In the research reported, roughly three topics were investigated: the properties of several graphene sources, the way to contact graphene on SiO_2 and finally the way to repeat this contacting on STO. The conclusions can be drawn and comments for further research are summarized below.

Graphene source

Mechanical exfoliation Mechanical exfoliation is used to obtain graphene samples. An investigation of several cleaning techniques showed that oxygen cleaning of the initial SiO_2 surface improves the substrate cleanness significantly. The use of IPA, acetone and THF to clean the graphene deposited does not result in a significant improvement of the graphene surface. Both clean graphene surfaces and relative dirty graphene flakes are observed at the same sample, suggesting the way they are produced differs. The difference is expected to be caused ny an other cleavage event occurring at the last exfoliation step: in case the graphite is cleaved during the last exfoliation step, the graphene area will be clean; however, in case the graphene is released from the tape in the last step, tape residue will be left on top of the graphene resulting in a significant lower surface quality.

CVD grown graphene CVD grown graphene on a nickel film is composed of single and multilayer flakes of graphene. As the amount of single layer graphene is minimal, this type of graphene source is not very efficient. CVD grown graphene on copper is investigated too. However, Raman spectroscopy showed that the bought sample did have a very low coverage of graphene. High quality samples of this type are promising candidates for graphene research.

Graphene transfer from a metal substrate As most CVD grown graphene is made using a transition metal as substrate, the method to transfer the graphene to a new surface is investigated. A high quality transfer method is developed which allows the transfer of graphene without having significant impact on the graphene quality. The final graphene quality is checked by Raman spectroscopy which showed a relative low amount of impurities.

Contacting graphene on SiO_2

Graphene deposited on SiO_2 by mechanical exfoliation is located using a marker field. A method is developed to write high resolution (300 nm sized) contacts on top of a flake. The electrical connection between the contacts and the flake is tested. IV-curves made at different back gate voltages showed no dependence of the conductivity on the gate voltage, so the measured flake was multilayer graphene. Its resistivity is estimated to be $3.2 \cdot 10^{-5}\,\Omega\cdot$m.

To contact graphene on STO

We have demonstrated that single layer graphene can be produced on STO by mechanical exfoliation. The low efficiency of this process and the charging of STO during electron beam lithography frustrate the contacting procedure. This can be solved by using a large area graphene source. After the transfer of large area, high quality, CVD grown graphene no alignment of the electron beam is required. This opens a new way that improves the efficiency and minimizes the inaccuracies introduced by electron beam lithography.

Appendix A

Gating graphene

This section discusses the important parameters playing a role in applying a back gate to graphene. First the influence of the back gate is explained, second the role of the dielectric is discussed. Finally the temperature dependance of the dielectric constant of STO is shown and its consequences are reported.

A.1 Back gate influence on electrical properties

Charge accumulation in the channel In a typical gating experiment, a conducting channel between source and drain is controlled by the gate voltage. The gate voltage needed to create a certain amount of charge in the conducting channel can be calculated via:

$$V_G = V_{CH} + Q \cdot \frac{d}{\varepsilon_{ins}\varepsilon_0} \tag{A.1}$$

V_G is the gate voltage, V_{CH} is the voltage at the channel side, d is the thickness and ε_{ins} is the dielectric constant of the insulator situated between the gate and the channel. In case V_G is applied with respect to V_{CH}, V_{CH} can be set to zero. So we can calculate the charge (and thus the carrier density) in the following way:

$$Q = V_G \cdot \frac{\varepsilon_{ins}\varepsilon_0}{d} \Rightarrow N = V_G \cdot \frac{\varepsilon_{ins}\varepsilon_0}{d \cdot e} \Rightarrow n = V_G \cdot \frac{\varepsilon_{ins}\varepsilon_0}{d \cdot e} \cdot \frac{1}{LWt} \tag{A.2}$$

where N is the amount of charge carriers, n is the charge carrier density, e is the electron charge and L, W, t are the length, width and thickness of the channel respectively. Additionally, via the resistivity ρ the mobility μ can be calculated:

$$\frac{1}{\rho} = ne\mu \Rightarrow \mu = \frac{d}{V_G \cdot \rho \cdot \varepsilon_{ins}\varepsilon_0} \tag{A.3}$$

This equation shows the direct relation of the dielectric insulator properties to the graphene channel.

A.2 $SrTiO_3$ as dielectric

Strontium titanate has dielectric constant which is heavily dependent on temperature. This is already mentioned in the introduction of this thesis and is

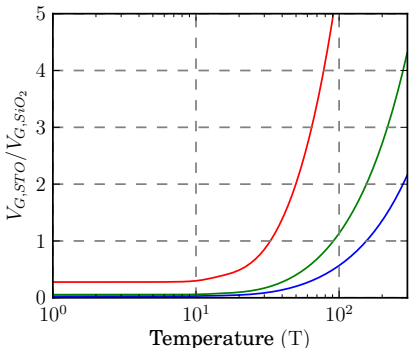

Figure A.1: Calculations on the ratio of the gate voltages for STO and SiO_2 as function of temperature at different STO thicknesses. The STO thicknesses used are: 50 μm (blue curve), 100 μm (green curve) and 500 μm (red curve).

shown in Fig. 1.2. This Figure is copied from [2] Their experimental data is fitted using the Barrett formula:

$$\varepsilon_{STO}(T) = \frac{C}{\frac{T1(T)}{2}\coth\frac{T1(T)}{2T} - Tc} \tag{A.4}$$

$T1(T)$ is given by

$$T1(T) = T1B2 + \frac{T1B1 - T1B2}{2}\left(1 + \tanh\frac{T - Tx}{\alpha}\right) \tag{A.5}$$

and the following constants: $C = 8 \cdot 10^4 K$, $Tc = 35.5K$, $T1B1 = 80K$, $T1B2 = 77.8K$, $Tx = 12K$ and $\alpha = 3.2K$ result in a high quality fit.

Using this formula, the behavior of the dielectric can be compared with the common used SiO_2. Most of the experiments on SiO_2 are performed using the following parameters: $d_{SiO_2} = 300\,\text{nm}$ and the V_G-range is $-80...80\,\text{V}$. The dielectric constant of SiO_2 is 3.9: $\varepsilon_{SiO_2} = 3.9$. As the limiting factor in our experiments is the gate voltage range we can apply, we have to calculate the ratio between the gate voltage in case of SiO_2 and the gate voltage in case of STO: V_{STO}/V_{SiO_2}. This has to be performed at different STO thicknesses and as function of temperature. The result of this calculation is shown in Fig. A.1. From this data it is clear that if the ratio of the gate voltages has to be kept below 2, the influence of the thickness of STO is not limiting the experiments below a temperature of 15 K. Due to the fact that 100 μm STO is quite fragile, an STO thickness between 200 and 500 μm is recommended.

Appendix B

Experimental procedures

All successful experimental procedures are listed here. They are described in quite a detail as a small change in the methods might have significant influence on the quality of the final result.

B.1 Graphene transfer and deposition

B.1.1 Mechanical Exfoliation

1. Take the sp-2 grade HOPG and remove the top layer by the Scotch tape. Discard the tape.
2. Take a piece of about 15 cm of Scotch tape and fold the very ends.
3. Put the clean part of the HOPG on the tape, turn over the tape and press it on top of the desk with the HOPG in between the tape and the desk.
4. Lift the HOPG using tweezers.
5. Fold and unfold the tape about 10 times while trying to obtain a uniform coverage of flakes.
6. Put the new substrate on a uniform and dense part of the tape.
7. Turn over the tape and uniformly press it on the table with the substrate in between.
8. Release the tape from the substrate while trying to keep the angle between the tape and the substrate as small as possible.

B.1.2 Transfer of CVD grown graphene on nickel or copper to SiO_2

Preparation of the etchant

Make a 0.5 M $FeCl_3$ and 0.01 M HCl solution in the following way:

1. Add 3.4 gr of $FeCl_3$ (hydrated) in 25 ml of de-ionized water.
2. Add one droplet of a 10× diluted 38% HCl-solution.

Substrate preparation

SiO_2

1. Take a $2 \times 2\,\mathrm{cm}^2$ piece of the silicon wafer (300nm SiO_2 on n-doped silicon).
2. Cut it into 4 pieces by a diamond pen. (Treat from bottom side!)
3. Put the substrates in acetone for 2 min.
4. Put the substrate in fresh acetone for 5 min in the sonicator.
5. Dip the substrates in IPA for 10 sec.
6. Put the substrate in fresh IPA for 5 min in the sonicator.
7. Actively blow away the solvent by dry N_2.
8. Put the substrates in the oxygen plasma cleaner: 1 min, 30 sccm, 100 W, 30 mTorr.

STO Extra care has to be taken into account when dealing with 100 μm thick STO: use glass plates to transport the sample.
The sample holder requires a $1 \times 1\,\mathrm{cm}^2$ substrate.

1. Let the STO slide from the package to a glass plate.
2. Clean the PEEK substrate holder (also inner side) with acetone and IPA, blow with N_2.
3. Let the STO slide from the glass plate onto the substrate holder.
4. Carefully center the sample.
5. Put the vacuum on the sample holder.
6. Blow the substrate with N_2.

Transfer procedure

1. Cut a piece of $1 \times 1\,\mathrm{cm}^2$ copper foil with a surgical blade on a hard underground; or take the Nickel sample.
2. For the copper film, if desired, reshape an edge to uniquely define the top and bottom side of the sample.
3. Coat the graphene-covered surface (sample) with about 300 nm PMMA-resist:
   - Put the sample at the spincoater and apply the vacuum.
   - Deposit two droplets of PMMA-495 and spin using the following parameters:
   - 1: RPM=500, ramp=5, TIME=3;
     2: RPM=4000, ramp=5, TIME=60
     3: RPM=4000, RAMP=5, TIME=0;
     4: RPM=3
   - Bake the sample for 1.5 min at 180 °C.
4. Copper: expose the uncovered side to oxygen plasma: 5 sec, 30 mTorr, 30 sccm, 100 W.
5. Coat the graphene-covered surface with about 40 μm SU8-resist:
   - Deposit more than enough resist on top.
   - 5 s at 500 rpm and 30 sec at 1500 rpm:
   - 1: RPM=500, RAMP=5, TIME=10;
     2: RPM=1500, RAMP=4,TIME=30;
     3: RPM=1500, RAMP=5, TIME=0;
     4: RPM=3
   - Bake the sample for at least 5 min at 90 °C.

6. Stick the resist-side of the sample to Scotch tape with a square opening in the center.
7. Dip the sample in the etchant for 45 min.
8. Dip the sample in a large beaker filled with de-ionized water for 2 min.
9. Dip the sample for 5 min in a 10× diluted 38% HCl solution.
10. Dip the sample in de-ionized water for 5 min.
11. Dry the sample with dry N_2.
12. Press the sample gently on top of a silicon wafer.
13. Put a droplet of acetone one the sample (using the pipette) and carefully pull away the tape.
14. Put the sample in acetone for 15 mins, the resist should be dissolved.
15. Put the sample in fresh acetone for 5 min.
16. Put the sample in IPA for 3 min.
17. Put the sample in fresh IPA for 3 min.
18. Blow-dry the sample with dry N_2.

B.2 Writing markers

In this section first the way to write a marker field is explained.

B.2.1 Exposure preparation

1. Prepare the substrate as explained in section B.1.2.
2. Deposit 2 à 3 droplets of MMA(8.5)MAA EL 9% and centrifuge for 5 sec at 500 rpm and 60 sec at 4000 rpm (recipe 2). (This should give a layer thickness of around 300 nm.)
3. Bake the substrate for 20 min at 170 °C.
4. Deposit 2 à 3 droplets of PMMA-950 A4 and centrifuge for 5 sec at 500 rpm and 60 sec at 4000 rpm (recipe 2). (This should result in a layer thickness of around 200 nm.)
5. Bake the substrate for 20 min at 170 °C.
6. Make a small scratch in the lower left corner of the substrate.

B.2.2 Exposure

Use a $400 \times 400\,\mu m^2$ writing field.

SiO_2

1. Write the markers with a dose of about $200\,\mu C/cm^2$, spot size 110 nm (PC9), writing time: 15 min.
2. Write the text (numbers) with a dose of about $200\,\mu C/cm^2$, dose factor $0.6 - 0.7$, spot size: 320 nm (PC4), writing time: 5 min.

STO

1. Try to use the lowest possible probe current (PC) to minimize charging problems. (PC13 was used during the focussing and alignment procedure.)
2. Define origin (global coordinate system) and try to focus on a particle (close to the edge will result in less charging problems).

3. Do the manual and automatic writefield alignment on a particle or on the edge of the sample.
4. Write the markers (large and small ones) using the following writing parameters:
   - Spot size: 110 nm (PC9)
   - Beam Current: 0.19 nA
   - Area Step Size: 0.038 μm
   - Area Dwell Time: 0.014 ms
   - Area Dose: 200 μC/cm^2
   - Beam Speed: 2.56 mm/s
5. Set PC4 and write the text (nubmers) using the following writing parameters:
   - Spot size: 320 nm (PC4)
   - Beam Current: 1.0 nA
   - Area Step Size: 0.158 μm
   - Area Dwell Time: 0.02 ms
   - Area Dose: 200 μC/cm^2 (Dose Factor: 0.7)
   - Beam Speed: 3.3 mm/s

B.2.3 Resist development

SiO_2

1. Put the substrate in MIBK:IPA (1:3) for 45 sec (90 sec for an undercut of about 500 nm).
2. Transfer the substrate to the IPA-develop solution immediately.
3. Wait for 45 sec and take out the substrate.
4. Actively blow the substrate with dry N_2.
5. Clean the substrate with an O_2-plasma for 100 sec (30 sccm, 100 W, 30 mTorr).

STO

1. Prepare the (cleaned) PEEK substrate holder.
2. Take the STO with a tweezer like you take it from the substrate holder (at one edge).
3. Dip the substrate in IPA:MIBK (1:3) and IPA (postdev) respectively, both for 60 sec.
4. Put the substrate on the substrate holder, apply vacuum, rinse the substrate with IPA and blow with N_2.

B.2.4 Metal evaporation

1. Mount the samples on the water cooled sample holder of the resistance evaporator.
2. Deposit 15 nm of Cr.
3. Deposit 35 nm of Au.

B.2.5 Lift off

1. Put the substrate in acetone for 30 min.

2. Add some fresh acetone to rinse the substrate.
3. Put the substrate in fresh acetone for 2 hours.
4. Put the substrate in IPA for 1 min.
5. Put the substrate in fresh IPA for 10 min.
6. Blow the substrate with N_2 (STO: use PEEK substrate holder).
7. SiO_2: clean the substrate with an O_2-plasma for 5 min (30 sccm, 100 W, 30 mTorr).

B.3 Contacting graphene on a SiO_2 and $SrTiO_3$ substrate using markers alignment.

The procedure to capture proper optical images is explained, the way how to import this in the EBPG software is given and finally the writing parameters are listed. This procedure is only tested for SiO_2. For STO, the optimal writing parameters to write the contacts is investigated only; the parameters used are given too. On STO, all the alignment and focussing is suggested to be performed using the lowest beam current which is going to be used (PC13).

Note that in this section, a global recipe and the writing parameters are listed only. The step-by-step procedure to write the structures using the electron beam lithography machine is listed in section B.4.4.

B.3.1 Identifying a graphene flake/position

1. Place the sample under the optical microscope:
   (a) Set the microscope to a low magnification.
   (b) Move the XY-stage to its origin.
   (c) Check that the image is not flipped/rotated.
   (d) Check that the $(0, 0)$-coordinate of the sample matches the center/origin of the microscope stage.
2. Take a picture at low magnification while the alignment markers are recognizable.
3. Measure the exact angle between the X-axes of the markers and the bottom of the picture (by the available software tool).
4. Find a graphene flake.
5. Take a picture of the flake in the highest possible magnification while still (at least) one marker is caught by the camera.
6. Correct the rotation to obtain a horizontal aligned picture using the software.
7. Crop the image to obtain at least one center of an alignment marker in a corner.
8. Save the image as bitmap with its magnification, the (XY)-coordinates of the lower left marker and the pixel size in its name.
9. Advise: Import the image in a word document and add an arrow pointing at the graphene flake to remember the exact location of this flake among all the other features present in the image.

B.3.2 Resist deposition

1. Deposit 2 à 3 droplets of MMA(8.5)MAA EL 9% and centrifuge for 5 sec at 500 rpm and 60 sec at 4000 rpm (recipe 2). (This should give a layer thickness of around 300 nm.)
2. Bake the sample for 20 min at 170 °C.
3. Deposit 2 à 3 droplets of PMMA-950 A4 and centrifuge for 5 sec at 500 rpm and 60 sec at 4000 rpm (recipe 2). (This should result in a layer thickness of around 200 nm.)
4. Bake the sample for 20 min at 170 °C.
5. Make a small scratch in the lower left corner of the sample using a diamond pen.

B.3.3 Importing images in the EBPG software

1. Conform the default .scc-file, create a .scc-file with the filename, the lower left and upper right corner coordinates and put it in the *Image*-directory.
2. Import the image in the lithography design via *(File→Import image)*, activate the design window and select *Show video* in the *Options* menu. After a zoom action, the image will appear.

B.3.4 Electron beam writing

In this section the most important steps are given to write structures by the EBPG. This procedure is quite global and can be used as a reminder for an advanced user. In this procedure, references are given to detailed step-by-step how-to's presented at the very end of this chapter (section B.4).

Exposure (preparation and writing)

1. Design the structure (Hall bars, traces and contact pads; for a detailed description: see B.4.1.)
2. Create the desired working areas. (For a detailed description: see B.4.2.)
3. Create or open an existing position list. (For a detailed description: see B.4.3.)
4. Do the alignment and write the designed structures using the following write and exposure settings. (For a detailed description: seeB.4.4.)

Settings optimized for SiO_2

For the large structures

- Spot size: 700 nm (PC1)
- Area dose: 200 μC/cm^2
- Area step size: 88 nm
- Settling time: *Manual*, 3 ms

The other parameters calculated by the software, will be something like:

- Beam current: 3.99 nA
- Area dwell time: 4 μs
- Beam speed 22.6 mm/s

For the small structures

- Spot size: 80 nm (PC10)
- Area dose: 200 μC/cm^2
- Area step size: 6 nm
- Settling time: Automatic

The other parameters calculated by the software, will be something like:

- Beam current: 0.03 nA
- Area dwell time: 3 μs
- Beam speed 2.5 mm/s (Don't let the beam speed exceed 5 mm/sec.)

Settings optimized for STO, only the small structures are tested

- Spot size: 41 nm (PC13)
- Dose: 200 μC/cm^2
- Area step size: 21.5 nm (or as small as possible)
- Area Dwell Time: 0.013ms (calculated by software)
- Beam Speed: 1.488 mm/s (calculated by software, don't let it exceed 5 mm/sec)
- Settling time: Automatic

B.3.5 Developing, metal evaporation, lift off

The development of the resist is equal to the marker writing case (see B.2.3), except the use of the O_2-plasma which has not to be applied as it will remove the graphene. The metal deposition is exactly the same as in the marker case (see B.2.4). Finally, the lift off is equal to the marker case (see B.2.5), but again the O_2-plasma treatment has to be skipped.

B.4 Detailed recipes to use the EBPG to contact graphene flakes

B.4.1 Drawing contacts

1. Select the proper writefield: $400 \times 400\,\mu$m^2 .
2. During drawing: do not cover an important alignment marker and try to keep the small traces within one stitch field.
3. Draw the desired structure/Hall bar in the right layer.
4. Add thin traces (500 nm) and increase their mutual distance as much as possible.
5. Draw traces using the *Open path* option, increase the width of the structure by double clicking on it.
6. Let no structures overlap and do not increase the width of the traces within a radius of 5 μm to the Hall bar.
7. On a second layer, place $100\times100\,\mu$m^2-sized squares close to the substrate edge, but be sure the resist quality is still good enough to write them. Place those pads as far from each other as possible to simplify future contacting. Also, try to keep all the structures belonging to one flake within one writefield.

8. Draw thick (10 μm) traces to connect the small traces and the large contact pads.
9. If the thickness of the large traces is less then 10 μm (or just for sure): use 30 μm-sized squares to be sure the large traces will be connected with the small ones.

B.4.2 Working area

Large structures

- Create separate working areas for each set of contacts belonging to a flake. So the amount of working areas will be the same as the amount of flakes.

Small structures

- If the writing time of all the small structures is short (<15 min), the working area can be the whole chip.
- If the writing time is longer, the working area has to be split. Dwell time corrections and automatic alignment steps have to be added to the position list in between each writing step.

B.4.3 Position list

Create separate position lists for the large and small contacts. They cannot be written automatically at once because some settings has to be manually adjusted (*Settling time*).

- Before each writing step: add an *Dwell time correction* entry and add several *Automatic Writefield Alignment* steps at wish.
- Check the settings for each writing step:
    1. The right working area.
    2. The right layers: check that the right automatic writefield alignment layers are selected.
    3. If no automatic writefield alignment is desired at each stitchfield of the working area, disable the automatic marks layer and add an alignment entry connected to a single writefield working area before the write entry.
    4. Click *Set Location*
    5. Have a look at the checkboxes of the exposure settings: they should be checked all.
- At the end of the position list, add a *Beam shutdown* entry.
- Save the position list.

B.4.4 Load, align, scan

1. Vent the EBPG, move the stage to the *Exchange Position*.
2. Place substrate on sample holder, close to the Faraday Cup.
3. Make a small (1 mm) scratch in the bottom left corner.
4. Blow the sample holder with N_2.
5. Pump down.
6. Move the stage to the (expected location of) the bottom left corner of the substrate.

7. After at least 5 min of pumping, select the smallest beam current which is going to be used and turn on *HV*.
8. Go to the bottom left corner of the substrate.
9. Adjust *Focus* (roughly).
10. Set the coordinate system to *Global*, set the origin $(0, 0)$ by clicking *Adjust*.
11. Move to the scratch, zoom in to find an isolated 1 μm sized particle.
12. Focus on the particle, double click in the image window to enter reduced area scan.
13. Do the *Manual Writefield Alignment*: $400 \times 400\,\mu\text{m}^2$, 5 μm particle.
14. Do the *Automatic Writefield Alignment*: $400 \times 400\,\mu\text{m}^2$, 5 μm particle.
15. Repeat the *Automatic Writefield Alignment* until the error is less then two digits (see the *Raith protocol software*).
16. Move the stage to the expected place of the bottom left *Global Marker* (e.g. move to $(1, 1)$).
17. Zoom in to have a maximum image width of 100 μm.
18. Zoom in and adjust *Focus*, use the reduced area scan by double clicking in the image window top optimize the focus.
19. Go to the 3-point correction tab and click on *Local* to enter the local coordinate system.
20. Move the center of the *Global Marker* to the center of the image window and read the (X, Y)-position for *Flag1*. Set the (U, V)-coordinates to the center of the *Global Marker* in the design.
21. Check the checkbox of *Flag1* to activate it.
22. Move the stage to the expected place of the second and third *Global Marker* and repeat the procedure.
23. The three checkboxes should have been checked. Click on *Adjust*.
24. Measure the *Beam Current* and adjust the *Exposure* and *Writing Settings* using the global *Calculator*. The relevant writing and exposure settings are listed in section B.3.4.
25. Scan a position lists that performs a *Automatic Marker Alignment* on a arbitrary stitchfield.
26. Check the error and repeat the scan until the error is small enough (1 or 2 digits).
27. Scan the position list belonging to the small structures.
28. Set the beam size for the large structures, wait for 5 min.
29. Go to the *Global* coordinate system, find the bottom left corner of the sample and adjust the origin.
30. Go to and refocus on a *Global Marker*.
31. Go to the *Local* coordinate system and perform the 3-point correction.
32. Do a *Manual Writefield Alignment* on a *Global Marker*.
33. Scan a position list that performs an *Automatic Marker Alignment* on an arbitrary stitchfield, repeat until an acceptable error (1 or 2 digits).
34. Scan the position list belonging to the large structures.
35. Check the *HV* to be off.
36. Move the stage to the *Exchange Position*.
37. Vent the system.
38. Unload the sample holder and evacuate the system.

Bibliography

[1] K. Novoselov, Nature Physics **2**, 177 (2006).

[2] K. Mueller, Physical Review B **19**, 3593 (1979).

[3] P. Blake, APL **91**, 063124 (2007).

[4] M. Pimenta, Phys Chem Chem Phys **9**, 1276 (2007).

[5] R. Saito, PRL **88** (2002).

[6] Y. Wang, J Phys Chem C **112**, 10637 (2008).

[7] K. Novoselov, Nature **438**, 197 (2005).

[8] K. Novoselov, PNAS **102**, 10451 (2005).

[9] *http://sciencewatch.com/ana/st/graphene/09febstgranovo/.*

[10] J. Li, L. Vandersypen and S. Goossens (private communication).

[11] R. Nair, Science **320**, 1308 (2008).

[12] E. Obraztsova, Phys Stat Sol (B) **245**, 2055 (2008).

[13] W. Bao, Nature Nanotechnology **4**, 562 (2009).

[14] X. Li, NanoLetters **10**, 4328 (2010).

[15] Q. Yu, Nature Materials **online**, 3010 (2011).

[16] C. Lui, Nature Letters **462**, 339 (2009).

[17] K. Kirshnan, Nature **144**, 667 (1939).

[18] S. Akcoltekin, Nanotechnology **20**, 155601 (2009).